The variational formulation of viscoplastic constitutive updates

Michael Ortiz, Laurent Stainier

The variational formulation of viscoplastic constitutive updates

M. Ortiz*, L. Stainier

Graduate Aeronautical Laboratories, California Institute of Technology, Pasadena, CA 91125, USA

We present a class of constitutive updates for general viscoplastic solids including such aspects of material behavior as finite elastic and plastic deformations, non-Newtonian viscosity, rate-sensitivity and arbitrary flow and hardening rules. The distinguishing characteristic of the proposed constitutive updates is that, by construction, the corresponding incremental stress–strain relations derive from a pseudo-elastic strain-energy density. This, in turn, confers the incremental boundary value problem a variational structure. In particular, the incremental deformation mapping follows from a minimum principle. This minimum principle may conveniently be taken as a basis for error estimation and mesh adaption. The accuracy and robustness of the variational constitutive updates is demonstrated with the aid of convergence tests involving the finitely-deforming Mises solid and ductile single crystals. The ability of the updates to resolve the complex patterns of slip activity which arise in the latter application is particularly noteworthy.

1. Introduction

The numerical integration of history-dependent constitutive relations plays a central role in computational plasticity. Considerable effort has been devoted to the formulation of constitutive updates which retain acceptable accuracy and efficiency over finite time steps. A widely used class of constitutive updates is the so-called return mapping algorithms. The essence of this approach dates back to the pioneering work of Wilkins [74], and has subsequently been extended to include non-smooth yield surfaces, such as arise in multi-surface plasticity, rate sensitivity and other aspects of material behavior [16,17,41,48–51,54,56,57,63–65]. Key mathematical tools which have aided these developments are convex analysis [20,43–46,48]; operator splitting and product formulae [48,50,54,57]; and nonlinear semi-group theory, specially as regards issues related to the analysis of consistency, stability and convergence [48,50,51,57]. Variational formulations for the elastoplastic boundary value problem have also been recently advanced [15,23,24]. These principles provide an effective basis for the formulation of mixed finite-element approximations, wherein both the displacement and the state-variable fields are represented by interpolation.

However, perhaps the most compelling aspect of variational formulations, specially when they take the form of a *minimum principle*, is that they provide a suitable basis for error estimation and, by extension, for mesh adaption in strongly nonlinear problems [58]. While methods of error estimation and mesh adaption for linear problems are presently well understood (e.g. [71]), they are comparatively less developed in the context of strongly nonlinear, possibly dynamic, problems [8,17,31,52]. Radovitzky and Ortiz [58] have recently shown that the solutions of the incremental boundary value problem for a wide class of materials, including nonlinear elastic solids, compressible Newtonian fluids, and viscoplastic solids, obey a minimum principle, even in the presence of inertia, provided that the constitutive updates are formulated appropriately. Under these conditions, the finite element error is bounded above by the corresponding interpolation error and, consequently, the

*Corresponding author. e-mail: ortiz@madrid.caltech.edu

classical interpolation-error bounds of approximation theory apply (e.g. [14]). The resulting error bounds in turn provide an effective framework for mesh adaption.

In this paper, we present a class of constitutive updates for general viscoplastic solids including such aspects of material behavior as finite elastic and plastic deformations, non-Newtonian viscosity, rate-sensitivity and arbitrary flow and hardening rules. The distinguishing characteristic of the proposed constitutive updates is that, by construction, the corresponding incremental stress–strain relations derive from a pseudo-elastic strain-energy density. While the focus of this work in on the time-integration of the constitutive relations, it follows immediately that the existence of a pseudo-elastic strain-energy density confers the incremental boundary value problem a variational structure. In particular, the incremental deformation mapping follows from a *minimum principle*.

As already mentioned, this minimum principle may be taken as a basis for error estimation and mesh adaption [58]. However, an essential difficulty in dealing with finitely deforming viscoplastic solids is that the incremental pseudo-elastic strain energy density is not convex in general [4], and often fails to be quasi-convex, e.g. due to latent hardening or to geometrical softening in single crystals [53]. This lack of quasi-convexity may give rise to arbitrarily fine oscillations in the solution (see e.g. [5,13]), which compounds matters of mesh adaption. However, Friesecke and Dolzmann [57] have shown that certain forms of viscosity regularize the problem and render the effective time-discretized energy density quasi-convex for sufficiently small time step. Similar conclusions were drawn by Needleman [47] as regards the stabilizing effect of rate-dependency in problems involving strain localization. These observations provide an incentive for the explicit consideration of viscosity and rate-sensitivity in the material description.

The constitutive framework adopted here is based on a conventional internal-variable formulation of continuum thermodynamics (see e.g. [33,34]). Within this framework, Coleman's relations characterize the equilibrium properties of the solid and the kinetics of the internal processes is described by a general set of rate equations. In particular, these rate equations account for the rate-sensitivity of the solid. In addition, we endow the solid with non-Newtonian viscosity. We note, however, that in order to describe general plastic flow rules, the conventional internal variable formalism must be extended so as to include non-holonomic internal constraints. We show that, for a given rate of deformation, the internal-variable rates and the direction of plastic flow, or flow rule, may jointly be derived from a variational principle which generalizes the principle of maximum dissipation. This variational characterization of the constitutive relations applies even in the presence of rate-sensitivity and non-Newtonian viscosity.

The cornerstone of the variational updates proposed here is a time-discretized version of the variational statement of the constitutive relations just described. We show that the minimization of a quasi-thermodynamic function, which combines the free energy of the solid, the conjugate inelastic potential for the kinetic equations and the viscous potential, jointly returns the updated value of the internal variables and the effective plastic flow direction, or flow rule, over the time step. In addition, we show that the minimum of the quasi-thermodynamic function thus obtained acts as a potential for the stress–strain relations, thus ensuring the variational character of the update. In particular, the consistent or algorithmic tangent moduli [66] are automatically symmetric.

The constitutive update is thus reduced to a nonlinear optimization problem for the updated internal variables and such kinematic parameters as determine the plastic flow direction. In the case of multi-surface plasticity, as exemplified by models of ductile single crystals, the determination of the active constraints becomes the central problem. A number of efficient nonlinear optimization techniques are presently in existence which furnish a systematic means of determining the active constraint set (see e.g. [9]). The accuracy and robustness of the variational constitutive updates is demonstrated with the aid of convergence tests for the finitely-deforming Mises solid and ductile single crystals. The ability of the updates to resolve the complex patterns of slip activity which arise in the latter case is particularly noteworthy.

2. General formulation of viscoplasticity

In order to narrow down the discussion, we begin by drawing a sharp distinction between internal processes whose kinetics involve gradients, e.g. heat conduction and diffusion, and internal processes which are ostensibly local. The former class of internal processes are governed by field equations such as the heat equation. We shall

presume that the multi-physics aspects of the problem are addressed by recourse to a staggered procedure [1,2,10,11,32,40], with the result that during a mechanical step the internal variables governed by nonlocal kinetics, such as temperature, entropy, or second-phase concentrations, are held fixed at known values. The problem is thus reduced to the integration of the constitutive equations which describe the local internal processes.

Our primary focus in the present paper concerns plastic and viscoplastic solids. These solids are characterized by the existence of a certain class of deformations $\boldsymbol{F}^{\mathrm{p}}$, or 'plastic' deformations, which leave the crystal lattice undistorted and unrotated, and, consequently, induce no long-range stresses. In addition to the plastic deformation $\boldsymbol{F}^{\mathrm{p}}$, some degree of lattice distortion $\boldsymbol{F}^{\mathrm{e}}$ may also be expected in general. One therefore has, locally,

$$\boldsymbol{F} = \boldsymbol{F}^{\mathrm{e}}\boldsymbol{F}^{\mathrm{p}} \tag{2.1}$$

This multiplicative elastic-plastic kinematics was first suggested by Lee [30] and further developed by others [3,25,26,37,60,68] within the context of ductile single crystals.

For purposes of illustration, we shall refer below to the linearization of (2.1). Let $\boldsymbol{u}$ be a displacement field about the undeformed configuration. Then, the linear part of the deformation gradient $\boldsymbol{F}$ about the undeformed configuration in the direction of $\boldsymbol{u}$ is (e.g. [38])

$$\langle D\boldsymbol{F}, \boldsymbol{u}\rangle = \nabla\boldsymbol{u} \equiv \boldsymbol{\beta} \tag{2.2}$$

The linearization of (2.1) is, therefore:

$$\boldsymbol{\beta} = \boldsymbol{\beta}^{\mathrm{e}} + \boldsymbol{\beta}^{\mathrm{p}} \tag{2.3}$$

where $\boldsymbol{\beta}^{\mathrm{e}}$ and $\boldsymbol{\beta}^{\mathrm{p}}$ are the linear parts of $\boldsymbol{F}^{\mathrm{e}}$ and $\boldsymbol{F}^{\mathrm{p}}$, respectively. The linearized strain tensor $\boldsymbol{\epsilon}$ is the symmetric part of $\boldsymbol{\beta}$. Likewise, the elastic and plastic strain tensors $\boldsymbol{\epsilon}^{\mathrm{e}}$ and $\boldsymbol{\epsilon}^{\mathrm{p}}$ are the symmetric parts of $\boldsymbol{\beta}^{\mathrm{e}}$ and $\boldsymbol{\beta}^{\mathrm{p}}$, respectively.

We adopt an internal variable formalism [33,34] to describe the local inelastic processes and postulate the existence of a Helmholtz free energy density of the form

$$A = A(\boldsymbol{F}^{\mathrm{e}}, \boldsymbol{F}^{\mathrm{p}}, \boldsymbol{Q}) = A(\boldsymbol{F}\boldsymbol{F}^{\mathrm{p}-1}, \boldsymbol{F}^{\mathrm{p}}, \boldsymbol{Q}) \equiv A(\boldsymbol{F}, \boldsymbol{F}^{\mathrm{p}}, \boldsymbol{Q}) \tag{2.4}$$

where $\boldsymbol{Q} \in R^{N}$ denotes some suitable collection of internal—or hardening—variables. The free energy may also depend on other variables, such as temperature, vacancy and solute concentrations, and others, whose evolution is governed by partial differential field equations. As remarked earlier, we presume such variables to be integrated independently as part of a staggered procedure and for present purposes they may be regarded as given. The complete set of internal variables is, therefore, $\{\boldsymbol{F}^{\mathrm{p}}, \boldsymbol{Q}\}$. The local *state* of the material is described by the variables $\{\boldsymbol{F}, \boldsymbol{F}^{\mathrm{p}}, \boldsymbol{Q}\}$.

We shall denote by $\boldsymbol{P}$ the first Piola–Kirchoff stress tensor (e.g. [38]). The equilibrium part of $\boldsymbol{P}$ follows from Coleman's relations as $A_{,\boldsymbol{F}}(\boldsymbol{F}, \boldsymbol{F}^{\mathrm{p}}, \boldsymbol{Q})$. The tacit assumption in writing (2.4) is that

$$A_{,\boldsymbol{F}}(\boldsymbol{F}^{\mathrm{e}} = \boldsymbol{I}, \boldsymbol{F}^{\mathrm{p}}, \boldsymbol{Q}) = \boldsymbol{0} \tag{2.5}$$

i.e. that the solid fully relaxes its free energy when its plastic deformation $\boldsymbol{F}^{\mathrm{p}}$ exactly matches the overall imposed deformation $\boldsymbol{F}$. However, the kinematics of plastic flow, as embodied in the plastic flow rule, generally results in incompatible plastic deformation fields. This incompatibility prevents the full plastic relaxation of the free energy and the material becomes stressed.

EXAMPLE 2.1: Structure-insensitive elastic response. In materials such as metals, the elastic response is ostensibly independent of the internal processes and the free energy (2.4) decomposes additively as

$$A = W^{\mathrm{e}}(\boldsymbol{F}\boldsymbol{F}^{\mathrm{p}-1}) + W^{\mathrm{p}}(\boldsymbol{F}^{\mathrm{p}}, \boldsymbol{Q}) \tag{2.6}$$

The function W^e determines the elastic response of the metal, e.g. upon unloading, whereas the function W^p describes the hardening of the material. Physically, W^p represents the stored energy due to the plastic working of the material. If W^p is independent of $\boldsymbol{F}^p$ and the state of hardening if fully described by a single internal variable, i.e. $N = 1$, then the material is said to undergo isotropic hardening. The case in which W^p depends on $\boldsymbol{F}^p$ only is known as kinematic hardening. The back-stress tensor:

$$\boldsymbol{T}_c = W^p_{,\boldsymbol{F}^p} \tag{2.7}$$

represents a shift in the plastic flow potential, or the elastic domain in the rate-independent limit.

EXAMPLE 2.2: Power-law hardening. The commonly employed isotropic hardening model assumes a power-law structure of the form:

$$W^p = Y_0 Q + \frac{nY_0Q_0}{n+1}\left(\frac{Q}{Q_0}\right)^{(n+1)/n} \tag{2.8}$$

where Y_0 and Q_0 are constants, and n is the hardening exponent.

If, in addition, the material possesses viscosity, the stresses follow in the form

$$\boldsymbol{P} = A_{,\boldsymbol{F}}(\boldsymbol{F}, \boldsymbol{F}^p, \boldsymbol{Q}) + \boldsymbol{P}^v(\dot{\boldsymbol{F}}; \boldsymbol{F}, \boldsymbol{Q}) \tag{2.9}$$

where $\boldsymbol{P}^v$ is the viscous part of the stresses. The viscosity law $\boldsymbol{P}^v(\dot{\boldsymbol{F}}; \boldsymbol{F}, \boldsymbol{Q})$ is said to derive from a potential if there exists a function $\phi(\dot{\boldsymbol{F}}; \boldsymbol{F}, \boldsymbol{Q})$ such that

$$\boldsymbol{P}^v = \phi_{,\dot{\boldsymbol{F}}}(\dot{\boldsymbol{F}}; \boldsymbol{F}, \boldsymbol{Q}) \tag{2.10}$$

We shall assume the usual regularity condition of P^v, namely, that

$$\boldsymbol{P}^v(\dot{\boldsymbol{F}}; \boldsymbol{F}, \boldsymbol{Q}) \cdot \dot{\boldsymbol{F}} = o(|\dot{\boldsymbol{F}}|) \tag{2.11}$$

where, here and subsequently, the dot product between two second-order tensors $\boldsymbol{A}$ and $\boldsymbol{B}$ is understood to be $\boldsymbol{A} \cdot \boldsymbol{B} \equiv A_{ij}B_{ij}$. The regularity condition (2.11) ensures that quasi-static processes do not result in viscous dissipation.

EXAMPLE 2.3: Newtonian viscosity. In the case of Newtonian viscosity, the viscous stresses follow as

$$\boldsymbol{P}^v = J\boldsymbol{\sigma}^v\boldsymbol{F}^{-T} \tag{2.12}$$

where

$$\boldsymbol{\sigma}^v = 2\eta\boldsymbol{d}^{dev} \tag{2.13}$$

is the viscous part of the Cauchy stress tensor. In this latter relation,

$$\boldsymbol{d} = \mathrm{sym}(\dot{\boldsymbol{F}}\boldsymbol{F}^{-1}) \tag{2.14}$$

is the rate of deformation tensor, $\boldsymbol{d}^{dev}$ is its deviatoric component, and η is the viscosity of the fluid. A simple calculation reveals that the Newtonian viscosity law possess the potential structure (2.10), and that the viscous potential is given by

$$\phi = \eta J\boldsymbol{d}^{dev} \cdot \boldsymbol{d}^{dev} \tag{2.15}$$

which is quadratic in $\dot{\boldsymbol{F}}$.

In order to determine the evolution of the internal variables, suitable kinetic equations must be supplied. Assuming that the rate of the local internal processes described by $\boldsymbol{Q}$ is determined solely by the local thermodynamic state, the general form of the kinetic equations is

$$\dot{\boldsymbol{Q}} = \boldsymbol{f}(\boldsymbol{F}, \boldsymbol{F}^{\mathrm{p}}, \boldsymbol{Q}) \tag{2.16}$$

In addition, the rate of plastic deformation $\dot{\boldsymbol{F}}^{\mathrm{p}}$ is subject to the kinematic restrictions imposed by a flow rule of the general form:

$$\dot{\boldsymbol{F}}^{\mathrm{p}}\boldsymbol{F}^{\mathrm{p}-1} = \dot{\boldsymbol{Q}}\boldsymbol{M}(\boldsymbol{K}) \tag{2.17}$$

where $\boldsymbol{K}$ is a set of additional kinematic variables, the significance of which will subsequently be clarified by way of example.

EXAMPLE 2.4: Tresca's flow rule. The kinematical basis of Tresca's plasticity theory is the assumption that there exists a pair of orthogonal unit vectors $\boldsymbol{s}$ and $\boldsymbol{m}$, or instantaneous slip system, such that the direction of the plastic deformation rate is:

$$\dot{\boldsymbol{F}}^{\mathrm{p}}\boldsymbol{F}^{\mathrm{p}-1} = \dot{\gamma}(\boldsymbol{s} \otimes \boldsymbol{m}) \tag{2.18}$$

where the rate $\dot{\gamma}$ is the slip rate on the instantaneous slip system $\{\boldsymbol{s}, \boldsymbol{m}\}$. In this example one has:

$$\boldsymbol{M} = \boldsymbol{s} \otimes \boldsymbol{m} \tag{2.19}$$

and the kinematic parameters $\boldsymbol{K}$ are simply the vectors $\boldsymbol{s}$ and $\boldsymbol{m}$.

EXAMPLE 2.5: von Mises' flow rule. A possible extension of von Mises' theory of plasticity to the finite deformation range is obtained by postulating a flow rule of the form:

$$\dot{\boldsymbol{F}}^{\mathrm{p}}\boldsymbol{F}^{\mathrm{p}-1} = \dot{\epsilon}^{\mathrm{p}}\boldsymbol{M} \tag{2.20}$$

where ϵ^{p} is the effective plastic strain and the matrix $\boldsymbol{M}$ is required to satisfy the incompressibility constraint:

$$\mathrm{trace}(\boldsymbol{M}) = 0 \tag{2.21}$$

and the normalization condition:

$$\boldsymbol{M} \cdot \boldsymbol{M} = \frac{3}{2} \tag{2.22}$$

but is otherwise unspecified. The normalization condition (2.22) is chosen so that $\dot{\epsilon}^{\mathrm{p}}$ coincides with the rate of axial stretching in the uniaxial test. The kinematic variable $\boldsymbol{K}$ coincides with $\boldsymbol{M}$. It follows that flow rule (2.20) specifies both the plastic rate of deformation tensor, $\mathrm{sym}(\dot{\boldsymbol{F}}^{\mathrm{p}}\boldsymbol{F}^{\mathrm{p}-1})$, and the plastic spin, $\mathrm{skew}(\dot{\boldsymbol{F}}^{\mathrm{p}}\boldsymbol{F}^{\mathrm{p}-1})$.

EXAMPLE 2.6: Single crystals. Plastic deformations in single crystals are crystallographic in nature. The conventional flow rule in this case is of the form [60]

$$\dot{\boldsymbol{F}}^{\mathrm{p}} = \left(\sum_{\alpha=1}^{N} \dot{\gamma}^{\alpha} \boldsymbol{s}^{\alpha} \otimes \boldsymbol{m}^{\alpha} \right) \boldsymbol{F}^{\mathrm{p}}$$

where γ^{α} is the slip strain, and $\boldsymbol{s}^{\alpha}$, and $\boldsymbol{m}^{\alpha}$ are orthogonal unit vectors defining the slip direction and slip-plane normal corresponding to slip system α. The collection $\boldsymbol{\gamma}$ of slip strains is part of the internal variable set $\boldsymbol{Q}$. A zero value of a slip rate $\dot{\gamma}^{\alpha}$ signifies that the corresponding slip system α is inactive. The flow rule (2.23) allows for multiple slip, i.e. for simultaneous activity on more than one system over a region of the crystal. The vectors $\{\boldsymbol{s}^{\alpha}, \boldsymbol{m}^{\alpha}\}$ remain constant throughout the deformation and are determined by crystallography. For instance, in f.c.c. crystals s^{α} is any cube face diagonal and m^{α} any cube diagonal. We therefore have:

$$\boldsymbol{M} = \{\boldsymbol{s}^{(1)} \otimes \boldsymbol{m}^{(1)}, \ldots, \boldsymbol{s}^{(N)} \otimes \boldsymbol{m}^{(N)}\}$$

and the parameter set $\boldsymbol{K}$ is empty. In the rate-independent limit, the elastic domain of a single crystal follows as the intersection of a finite collection of half-spaces. Therefore, single crystals furnish a convenient—and technologically important—example of multi-surface plasticity.

The general structure of the kinetic equations (2.16) and the flow rule (2.17) merits further discussion. These equations may jointly be written in differential form as

$$\begin{pmatrix} \boldsymbol{I} & -(\boldsymbol{M}\boldsymbol{F}^{\mathrm{p}})^{\mathrm{T}} \\ \boldsymbol{0} & \boldsymbol{I} \end{pmatrix} \mathrm{d}\begin{Bmatrix} \boldsymbol{F}^{\mathrm{p}} \\ \boldsymbol{Q} \end{Bmatrix} + \begin{Bmatrix} \boldsymbol{0} \\ -\boldsymbol{f} \end{Bmatrix} \mathrm{d}t = \begin{Bmatrix} \boldsymbol{0} \\ \boldsymbol{0} \end{Bmatrix} \tag{2.25}$$

These relations may be regarded as a set of *non-holonomic* constraints operating on the full internal variable set $\{\boldsymbol{F}^{\mathrm{p}}, \boldsymbol{Q}\}$. In the context of structural mechanics, this view has been developed by [69,70,72]. We also note that the kinematic parameters $\boldsymbol{K}$ could in principle be eliminated from (2.17), leading to non-holonomic constraints of the form:

$$\boldsymbol{g}(\dot{\boldsymbol{F}}^{\mathrm{p}}\boldsymbol{F}^{\mathrm{p}-1}, \dot{\boldsymbol{Q}}) = \boldsymbol{0} \tag{2.26}$$

where the constraint function $\boldsymbol{g}$ is homogeneous of degree one in the rates $\{\dot{\boldsymbol{F}}^{\mathrm{p}}, \dot{\boldsymbol{Q}}\}$.

EXAMPLE 2.7: von Mises' flow rule. The kinematic matrix $\boldsymbol{M}$ may be eliminated from flow rule (2.20) by recourse to the normalization condition (2.22), with the result:

$$g = \|\dot{\boldsymbol{F}}^{\mathrm{p}}\boldsymbol{F}^{\mathrm{p}-1}\| - \frac{3}{2}|\dot{\epsilon}^{p}| = 0 \tag{2.27}$$

where $\|\boldsymbol{A}\| \equiv \sqrt{\boldsymbol{A}\cdot\boldsymbol{A}}$.

However, the resulting constraint functions may be cumbersome and it is often advantageous to work with a parameterized flow rule of the form (2.17). The variational statement of the constitutive relations given in Section 3 may then be invoked in order to *optimize* the parameters $\boldsymbol{K}$. As we shall see, by an appropriate choice of parameterization this approach leads to such conventional flow rules as Tresca's and von Mises'.

The thermodynamic force conjugate to $\boldsymbol{F}^{\mathrm{p}}$ is

$$\boldsymbol{T} = -A_{,\boldsymbol{F}^{\mathrm{p}}} \tag{2.28}$$

Correspondingly, the thermodynamic force conjugate to $\boldsymbol{Q}$ is

$$\boldsymbol{Y} = \boldsymbol{T}(\boldsymbol{M}\boldsymbol{F}^{\mathrm{p}}) - A_{,\boldsymbol{Q}} \tag{2.29}$$

where we have accounted for the fact that, in view of the flow rule (2.17), a variation in $\boldsymbol{Q}$ necessarily implies a variation in $\boldsymbol{F}^{\mathrm{p}}$.

EXAMPLE 2.8: Structure-insensitive elastic response. For solids possessing a free energy with the structure (2.6) and exhibiting kinematic hardening, i.e. a dependence of W^{p} on $\boldsymbol{F}^{\mathrm{p}}$, the thermodynamic force conjugate to $\boldsymbol{F}^{\mathrm{p}}$ follows from (2.28) and (2.7) in the form:

$$\boldsymbol{T} = \boldsymbol{F}^{\mathrm{e}^{\mathrm{T}}}\boldsymbol{P} - \boldsymbol{T}_{c} \tag{2.30}$$

whence it is seen that $\boldsymbol{T}_{c}$ does indeed act as a back-stress.

EXAMPLE 2.9: Isotropic Tresca's model. In the case of Tresca's flow rule (2.18) and an isotropically hardening material, the thermodynamic driving force acting on the instantaneous slip strain rate follows from the general expression (2.29) in the form:

$$Y = \tau - \tau_c \tag{2.31}$$

where

$$\tau = (\boldsymbol{F}^{e^T}\boldsymbol{P}\boldsymbol{F}^{p^T}) \cdot (\boldsymbol{s} \otimes \boldsymbol{m}) \tag{2.32}$$

is the resolved shear stress on the plane of normal $\boldsymbol{m}$ in the direction $\boldsymbol{s}$, and

$$\tau_c = W^{p\prime}(\gamma) \tag{2.33}$$

is the shear flow stress.

EXAMPLE 2.10: Isotropic von Mises' model. For an isotropically hardening material obeying the finite deformation extension (2.20) of von Mises flow rule, the thermodynamic driving force (2.29) reduces to:

$$Y = \sigma - \sigma_c \tag{2.34}$$

where

$$\sigma = (\boldsymbol{F}^{e^T}\boldsymbol{P}\boldsymbol{F}^{p^T}) \cdot \boldsymbol{M} \tag{2.35}$$

is the equivalent uniaxial stress and

$$\sigma_c = W^{p\prime}(\epsilon^p) \tag{2.36}$$

is the uniaxial flow stress.

EXAMPLE 2.11: Single crystals. For a single crystal possessing a structure independent elastic response, Eq. (2.6), the thermodynamic driving force acting on slip system α is:

$$Y^\alpha = \tau^\alpha - \tau_c^\alpha \tag{2.37}$$

where

$$\tau^\alpha = (\boldsymbol{F}^{e^T}\boldsymbol{P}\boldsymbol{F}^{p^T}) \cdot (\boldsymbol{s}^\alpha \otimes \boldsymbol{m}^\alpha) \tag{2.38}$$

is the resolved shear stress on the plane of normal $\boldsymbol{m}^\alpha$ in the direction $\boldsymbol{s}^\alpha$, and

$$\tau_0^\alpha = W^p_{,\gamma^\alpha}(\boldsymbol{\gamma}) \tag{2.39}$$

is the critical resolved shear stress of system α. The hardening relations (2.39) may be expressed in rate form as

$$\dot{\tau}_0^\alpha = \sum_{\beta=1}^{N} h^{\alpha\beta}(\boldsymbol{\gamma})\dot{\gamma}^\beta$$

where

$$h^{\alpha\beta} = W^p_{,\gamma^\alpha\gamma^\beta}(\boldsymbol{\gamma})$$

is the hardening matrix of the crystal.

EXAMPLE 2.12: Latent hardening. Many of the intricacies in the behavior of single crystals, such as the development of certain micro-structures, may be traced to the phenomenon of latent hardening [17,18,53]. In many crystals, it is found that activity in a slip system hardens other systems more than it hardens the system itself [6,7,21,28,29,59]. Ortiz and Repetto [53] have devised a simple model of latent hardening based on two premises: (i) a parabolic hardening in single slip; (ii) off-diagonally dominant hardening matrix. A simple form of W^p consistent with these assumptions is

$$W^p = \sum_{\alpha=1}^{N} \tau_{c0}^\alpha \gamma^\alpha + \frac{n}{n+1}\tau_0\gamma_0\left(\frac{\gamma}{\gamma_0}\right)^{(n+1)/n} \tag{2.42}$$

where τ_{c0}^α is the initial critical resolved shear stress in slip system α, τ_0 is reference resolved shear stress, γ_0 is a reference slip strain, $a^{\alpha\beta}$ is a matrix of interaction coefficients, n is a hardening exponent, and

$$\gamma = \left(\sum_{\alpha=1}^{N} \sum_{\beta=1}^{N} a^{\alpha\beta} \gamma^{\alpha} \gamma^{\beta} \right)^{1/2} \tag{2.43}$$

is an effective slip strain. Parabolic hardening is obtained by setting $n = 2$. For crystal classes in which all slip systems are of the same crystallographic type, the diagonal components $a^{\alpha\alpha}$ of the interaction matrix may be normalized to unity without loss of generality. In the linear case, $n = 1$, the hardening matrix (2.41) evaluates to:

$$h^{\alpha\beta} = h_0 a^{\alpha\beta} \tag{2.44}$$

where $h_0 = \tau_0 / \gamma_0$. The latent hardening ratio (LHR) between systems α and β is then

$$\text{LHR} \equiv \frac{h^{\alpha\beta}}{h^{\alpha\alpha}} = \frac{a^{\alpha\beta}}{a^{\alpha\alpha}} \tag{2.45}$$

The LHR has often been taken to be constant and independent of the pair of interacting systems [55]. A commonly adopted value for f.c.c. crystals is LHR = 1.4.

The kinetic relations (2.16) are said to derive from an inelastic potential if there exists a differentiable function $\psi(\boldsymbol{Y})$ such that

$$\dot{\boldsymbol{Q}} = \psi_{,\boldsymbol{Y}}(\boldsymbol{Y}) \tag{2.46}$$

Additionally, we may introduce the dual potential $\psi^*(\dot{\boldsymbol{Q}})$ by recourse to the Legendre transformation

$$\psi^*(\dot{\boldsymbol{Q}}) = \boldsymbol{Y} \cdot \dot{\boldsymbol{Q}} - \psi(\boldsymbol{Y}) \tag{2.47}$$

Then, one has

$$\boldsymbol{Y} = \psi^*_{,\dot{\boldsymbol{Q}}}(\dot{\boldsymbol{Q}}) \tag{2.48}$$

which constitutes a restatement of the kinetic equations (2.46). Eq. (2.48) embodies both the hardening relations, through the dependence of $\boldsymbol{Y}$ on $\boldsymbol{Q}$, and the rate-sensitivity law. For single crystals, the concept of inelastic potential was introduced by Rice [61].

EXAMPLE 2.13: Power-law rate sensitivity. A frequently employed class of kinetic equations is obtained by postulating a power-law relation between each of the internal variable rates $\dot{\boldsymbol{Q}}$ and its corresponding thermodynamic force, which leads to a flow potential of the form:

$$\psi = \sum_{\alpha} \frac{Y_0 \dot{Q}_0}{m+1} \left(\frac{\max\{0, Y^{\alpha}\}}{Y_0} \right)^{m+1} \tag{2.49}$$

where Y_0 and $\dot{Q}_0$ are constants and m is the rate sensitivity exponent. The corresponding dual potential is:

$$\psi^* = \sum_{\alpha} \frac{m Y_0 \dot{Q}_0}{m+1} \left(\frac{\dot{Q}^{\alpha}}{\dot{Q}_0} \right)^{(m+1)/m} \qquad \dot{Q}^{\alpha} \geq 0 \tag{2.50}$$

$$\psi^* = \infty \qquad \dot{Q}^{\alpha} < 0 \tag{2.51}$$

We note that (2.51) constraints the internal variable rates to be in the range $\dot{Q}^{\alpha} \geq 0$.

The preceding constitutive relations are subject to material frame indifference, i.e. must remain invariant under superimposed rigid body motions.

3. Variational form of the constitutive relations

We proceed to develop a variational restatement of the above constitutive relations which will subsequently provide the basis for the formulation of variational updates. To this end we introduce the function:

$$D(\dot{\boldsymbol{F}}, \dot{\boldsymbol{Q}}; \boldsymbol{K}) = A_{,\boldsymbol{F}} \cdot \dot{\boldsymbol{F}} - \boldsymbol{Y} \cdot \dot{\boldsymbol{Q}} + \psi^*(\dot{\boldsymbol{Q}}) + \phi(\dot{\boldsymbol{F}}) \tag{3.1}$$

where all state functions are evaluated at the current state $\{\boldsymbol{F}, \boldsymbol{F}^{\mathrm{p}}, \boldsymbol{Q}\}$. It should be noted that the flow rule (2.17) is built into D through $\boldsymbol{Y}$, Eq. (2.29).

It is evident from this definition that the dual form (2.48) of the kinetic relations is recovered by optimizing D with respect to the rates $\dot{\boldsymbol{Q}}$. Indeed, the corresponding Euler equation is (2.48), i.e.

$$D_{,\dot{\boldsymbol{Q}}} = \psi^*_{,\dot{\boldsymbol{Q}}} - \boldsymbol{Y} = 0 \tag{3.2}$$

In addition, we shall optimize D with respect to the kinematic parameters $\boldsymbol{K}$, which leads to the variational principle:

$$\min_{\dot{\boldsymbol{Q}}, \boldsymbol{K}} D(\dot{\boldsymbol{F}}, \dot{\boldsymbol{Q}}; \boldsymbol{K}) \equiv D^{\mathrm{eff}}(\dot{\boldsymbol{F}}) \tag{3.3}$$

In this approach, it is incumbent upon the variational principle (3.3) to determine the *optimal* kinematic variables $\boldsymbol{K}$. This optimization in turn renders the flow rule determinate. Since D depends on $\boldsymbol{K}$ only through the term $\boldsymbol{T}(\boldsymbol{M}\boldsymbol{F}^{\mathrm{p}})$ in $\boldsymbol{Y}$, the minimization of D with respect to $\boldsymbol{K}$ is equivalent to the problem:

$$\max_{\boldsymbol{K}} \boldsymbol{T}[\boldsymbol{M}(\boldsymbol{K})\boldsymbol{F}^{\mathrm{p}}] \cdot \dot{\boldsymbol{Q}} \tag{3.4}$$

which may be regarded as a statement of the principle of maximum plastic dissipation (e.g. [35]). It also follows from (3.3) that

$$\boldsymbol{P} = D^{\mathrm{eff}}_{,\dot{\boldsymbol{F}}} = A_{,\boldsymbol{F}} + \phi_{,\dot{\boldsymbol{F}}} \tag{3.5}$$

i.e. $D^{\mathrm{eff}}(\dot{\boldsymbol{F}})$ acts as a rate-potential for the stresses $\boldsymbol{P}$. Next we show that the familiar flow rules of classical plasticity are indeed recovered from the preceding variational principle.

EXAMPLE 3.1: Tresca's solid. For a Tresca solid, the flow rule is given by (2.18) in terms of the kinematical parameters $\boldsymbol{s}$ and $\boldsymbol{m}$. The instantaneous value of these variables follows from the maximum principle (3.4), which specializes to

$$\max_{\boldsymbol{s}, \boldsymbol{m}} (\boldsymbol{T}\boldsymbol{F}^{pT}) \cdot (\boldsymbol{s} \otimes \boldsymbol{m}) \tag{3.6}$$

$$\text{subject to: } \|\boldsymbol{s}\| = \|\boldsymbol{m}\| = 1, \quad \boldsymbol{s} \cdot \boldsymbol{m} = 0 \tag{3.7}$$

In order to interpret this rule, it proves convenient to introduce the stress tensor:

$$\boldsymbol{S} = \boldsymbol{T}\boldsymbol{F}^{\mathrm{pT}} \tag{3.8}$$

Then, the vectors $\boldsymbol{s}$ and $\boldsymbol{m}$ define simply the direction and the plane of maximum shear corresponding to $\boldsymbol{S}$, and the resolved shear stress (2.32) is the attendant maximum resolved shear stress. Evidently, in the context of linearized kinematics $\boldsymbol{S}$ reduces to the Cauchy stress tensor $\boldsymbol{\sigma}$ and the familiar formulation of Tresca's theory is recovered.

EXAMPLE 3.2: Mises solid. The extension of von Mises' theory to finite deformations formulated in the foregoing is amenable to a similar treatment. The instantaneous value of the plastic deformation rate direction $\boldsymbol{M}$ follows from the maximum principle (3.4), which specializes to:

$$\max_{\boldsymbol{M}} (\boldsymbol{T}\boldsymbol{F}^{\mathrm{pT}}) \cdot \boldsymbol{M} \tag{3.9}$$

$$\text{subject to: } \mathrm{trace}(\boldsymbol{M}) = 0, \quad \boldsymbol{M} \cdot \boldsymbol{M} = \frac{3}{2} \tag{3.10}$$

The solution of this problem is

$$\boldsymbol{M} = \frac{3}{2}\frac{\boldsymbol{S}^{\mathrm{dev}}}{\sigma} \tag{3.11}$$

where

$$\sigma = \sqrt{\frac{3}{2}\boldsymbol{S}^{\mathrm{dev}} \cdot \boldsymbol{S}^{\mathrm{dev}}} \tag{3.12}$$

is the effective uniaxial stress. As before, in the context of linearized kinematics $\boldsymbol{S}$ reduces to the Cauchy stress tensor $\boldsymbol{\sigma}$ and the classical von Mises flow rule

$$\dot{\boldsymbol{\epsilon}}^{\mathrm{p}} = \dot{\epsilon}^{p}\frac{3}{2}\frac{\boldsymbol{\sigma}^{\mathrm{dev}}}{\sigma} \tag{3.13}$$

is recovered.

4. Constitutive updates

Next, we address the time-integration of the constitutive equations (2.9) and (2.16). In particular, we seek to formulate constitutive updates possessing an incremental potential structure, i.e. updates such that the incremental stress-deformation relations derive from a potential. As remarked in the introduction, this potential structure facilitates error estimation [58] and ensures that the tangent stiffness matrix is symmetric. A stress update having the requisite potential structure may be obtained by integration of the constitutive relations along 'minimizing paths', i.e. along such deformation histories as minimize the incremental work of deformation. The work of deformation itself then supplies the sought strain energy potential. This approach has been used in the past to derive deformation, or pseudo-elastic, theories of plasticity [12,36,39,49,67]. A recent application of minimizing paths to the study of dislocation structures in ductile single crystals may be found in [53]. However, the task of determining minimizing paths for specific models is often daunting, specially for rate-sensitive materials, which detracts from the practicality of the approach. Here, we give an alternative and more direct method for formulating updates possessing the requisite potential structure.

We envision an incremental solution procedure and concern ourselves with a generic time interval $[t_n, t_{n+1}]$. Let the initial state $(\boldsymbol{F}_n, \boldsymbol{F}^{\mathrm{p}}_n, \boldsymbol{Q}_n)$ and the updated deformations $\boldsymbol{F}_{n+1}$ be given. The first step in effecting an integration of the constitutive relations is to provide an incremental rule for updating $\boldsymbol{F}^{\mathrm{p}}$ in a manner compatible with the flow rule (2.17). We take this rule to be of the form:

$$\boldsymbol{F}^{\mathrm{p}}_{n+1} = \exp\{\Delta\boldsymbol{Q}\,\boldsymbol{M}(\boldsymbol{K})\}\boldsymbol{F}^{\mathrm{p}}_n \tag{4.1}$$

where $\exp(\cdot)$ denotes the exponential mapping for square matrices, and

$$\Delta\boldsymbol{Q} = \boldsymbol{Q}_{n+1} - \boldsymbol{Q}_n \tag{4.2}$$

By the properties of the exponential mapping, the update (4.1) satisfies the condition

$$\left[\frac{\mathrm{d}}{\mathrm{d}\lambda}\exp\{\lambda\,\Delta\boldsymbol{Q}\,\boldsymbol{M}(\boldsymbol{K})\}\right]_{\lambda=0^+} = \Delta\boldsymbol{Q}\,\boldsymbol{M}(\boldsymbol{K}) \tag{4.3}$$

which establishes the consistency of (4.1) with (2.17).

The exponential mapping has been applied to the integration of finite-deformation flow rules by Weber and Anand [73], Eterovic and Bathe [19], Cuitiño and Ortiz [16], Miehe and Stein [42] and Miehe [41]. A particularly appealing aspect of the exponential mapping is that it satisfies exactly the finite-deformation extension of kinematic constraints operating on $\boldsymbol{M}$. For instance, if $\boldsymbol{M}$ is traceless, in keeping with plastic incompressibility, then the plastic deformation $\boldsymbol{F}^{\mathrm{p}}_{n+1}$ computed through (4.1) has a determinant of one, as required.

EXAMPLE 4.1: Flow-rule update for the Tresca solid. The flow-rule update (4.1) for a Tresca solid takes the particularly simple form:

$$\boldsymbol{F}^{\mathrm{p}}_{n+1} = \exp\{\Delta\gamma\, \boldsymbol{s} \otimes \boldsymbol{m}\}\boldsymbol{F}^{\mathrm{p}}_{n} = (\boldsymbol{I} + \Delta\gamma\, \boldsymbol{s} \otimes \boldsymbol{m})\boldsymbol{F}^{\mathrm{p}}_{n} \tag{4.4}$$

which follows from the orthogonality of $\boldsymbol{s}$ and $\boldsymbol{m}$.

EXAMPLE 4.2: Flow-rule update for the Mises solid. For a Mises solid, the exponential update of (2.20) leads to:

$$\boldsymbol{F}^{\mathrm{p}}_{n+1} = \exp\{\Delta\epsilon^{p}\boldsymbol{M}\}\boldsymbol{F}^{\mathrm{p}}_{n} \equiv \boldsymbol{A}(\Delta\epsilon^{p})\boldsymbol{F}^{\mathrm{p}}_{n} \tag{4.5}$$

Evidently, $\boldsymbol{A}(\Delta\epsilon^{\mathrm{p}})$ may be taken to be any matrix satisfying the incompressibility constraint:

$$\det(\boldsymbol{A}) = 1 \tag{4.6}$$

The corresponding increment $\Delta\epsilon^{p}$ in the effective plastic strain follows from the normalization condition (2.22) as

$$\Delta\epsilon^{\mathrm{p}} = \sqrt{\frac{2}{3}}\,\|\log(\boldsymbol{A})\| \tag{4.7}$$

where $\log(\cdot)$ is the logarithmic mapping for square matrices.

EXAMPLE 4.3: Flow-rule update for crystals. For single crystals, the exponential update of (2.23) yields:

$$\boldsymbol{F}^{\mathrm{p}}_{n+1} = \exp\left\{\sum_{\alpha=1}^{N} \Delta\gamma^{\alpha}\boldsymbol{s}^{\alpha} \otimes \boldsymbol{m}^{\alpha}\right\}\boldsymbol{F}^{\mathrm{p}}_{n} \tag{4.8}$$

This update has been used by Ortiz and Repetto [53] to effect a time-discretization of the rate equations of single crystal plasticity.

Suppose that the kinetic equations and the viscosity law possess a potential structure such as expressed in Eqs. (2.46) and (2.10). A class of variational constitutive updates can then be modeled after the rate variational principle (3.3). In particular, we seek to characterize the updated internal variables $\boldsymbol{Q}_{n+1}$ and the kinematic variables $\boldsymbol{K}$ which determine $\boldsymbol{F}^{\mathrm{p}}_{n+1}$ as *minimizers* of a suitably chosen function. To this end, we define the incremental energy density as

$$W(\boldsymbol{F}_{n+1}; \boldsymbol{F}_{n}, \boldsymbol{Q}_{n}) = \Delta t\, \phi\left(\frac{\boldsymbol{F}_{n+1} - \boldsymbol{F}_{n}}{\Delta t}; \boldsymbol{F}_{n+\alpha}\right) + \min_{\boldsymbol{Q}_{n+1}, \boldsymbol{K}} \left\{A(\boldsymbol{F}_{n+1}, \boldsymbol{F}^{\mathrm{p}}_{n+1}, \boldsymbol{Q}_{n+1}) - A(\boldsymbol{F}_{n}, \boldsymbol{F}^{\mathrm{p}}_{n}, \boldsymbol{Q}_{n}) + \Delta t\, \psi^{*}\left(\frac{\boldsymbol{Q}_{n+1} - \boldsymbol{Q}_{n}}{\Delta t}, \boldsymbol{Q}_{n+\alpha}\right)\right\} \tag{4.9}$$

where it is tacitly understood that $\boldsymbol{F}^{\mathrm{p}}_{n+1}$ is computed through (4.1), and we write

$$\boldsymbol{F}_{n+\alpha} = (1 - \alpha)\boldsymbol{F}_{n} + \alpha\boldsymbol{F}_{n+1} \tag{4.10}$$

$$\boldsymbol{Q}_{n+\alpha} = (1 - \alpha)\boldsymbol{Q}_{n} + \alpha\boldsymbol{Q}_{n+1} \tag{4.11}$$

in terms of an algorithmic parameter $\alpha \in [0, 1]$. Evidently, the choice of incremental energy density W is not unique. The particular form (4.9) adopted here is motivated by the midpoint rule for numerical integration (e.g. [27]).

The optimality condition for the kinematic variables $\boldsymbol{K}$ is

$$W_{,\boldsymbol{K}} = -\boldsymbol{T}_{n+1}[\exp\{\Delta\boldsymbol{Q}\,\boldsymbol{M}(\boldsymbol{K})\}]_{,\boldsymbol{K}}\boldsymbol{F}^{\mathrm{p}}_{n} = \boldsymbol{0} \tag{4.12}$$

But letting $\Delta t \to 0$ and using the consistency (4.3) of the flow rule update gives

$$\lim_{\Delta t \to 0} W_{,\boldsymbol{K}} = -\boldsymbol{T}_{n}\,\Delta\boldsymbol{Q}[\boldsymbol{M}(\boldsymbol{K})]_{,\boldsymbol{K}}\boldsymbol{F}^{\mathrm{p}}_{n} = \boldsymbol{0} \tag{4.13}$$

which establishes consistency with the maximum principle (3.4). Effecting the minimization with respect to $\boldsymbol{Q}_{n+1}$ in (4.9), letting $\Delta t \to 0$ and using (4.13) gives the identity:

$$\boldsymbol{Y}_n = \psi^*_{,\dot{\boldsymbol{Q}}}(\dot{\boldsymbol{Q}}_n, \boldsymbol{Q}_n) \tag{4.14}$$

which demonstrates consistency with the dual form (2.48) of the kinetic relations. This completes the proof of consistency of the variational update with the constitutive relations.

Imagine now perturbing $\boldsymbol{F}_{n+1} \to \boldsymbol{F}_{n+1} + \delta\boldsymbol{F}_{n+1}$. The corresponding variation of W is

$$\delta W = \left\{ A_{,\boldsymbol{F}}(\boldsymbol{F}_{n+1}, \boldsymbol{F}^{\mathrm{p}}_{n+1}, \boldsymbol{Q}_{n+1}) + \boldsymbol{P}^{\mathrm{v}}\left(\frac{\boldsymbol{F}_{n+1} - \boldsymbol{F}_n}{\Delta t}; \boldsymbol{F}_{n+\alpha} \right) \right\} \cdot \delta\boldsymbol{F}_{n+1} + W_{,\boldsymbol{Q}_{n+1}} \cdot \delta\boldsymbol{Q}_{n+1} + W_{,\boldsymbol{K}} \cdot \delta\boldsymbol{K} \tag{4.15}$$

But the last two terms vanish by virtue of the stationarity condition of W with respect to $\{\boldsymbol{Q}_{n+1}, \boldsymbol{K}\}$, and (4.15) reduces to:

$$\delta W = \left\{ A_{,\boldsymbol{F}}(\boldsymbol{F}_{n+1}, \boldsymbol{F}^{p}_{n+1}, \boldsymbol{Q}_{n+1}) + \boldsymbol{P}^{\mathrm{v}}\left(\frac{\boldsymbol{F}_{n+1} - \boldsymbol{F}_n}{\Delta t}; \boldsymbol{F}_{n+\alpha} \right) \right\} \cdot \delta\boldsymbol{F}_{n+1} \tag{4.16}$$

Setting

$$\boldsymbol{P}_{n+1} = A_{,\boldsymbol{F}}(\boldsymbol{F}_{n+1}, \boldsymbol{F}^{\mathrm{p}}_{n+1}, \boldsymbol{Q}_{n+1}) + \boldsymbol{P}^{\mathrm{v}}\left(\frac{\boldsymbol{F}_{n+1} - \boldsymbol{F}_n}{\Delta t}; \boldsymbol{F}_{n+\alpha} \right) \tag{4.17}$$

which is clearly consistent with (2.9), Eq. (4.16) adopts to form:

$$\delta W = \boldsymbol{P}_{n+1} \cdot \delta\boldsymbol{F}_{n+1} \tag{4.18}$$

But, since $\delta\boldsymbol{F}_{n+1}$ is arbitrary, this identity implies that

$$\boldsymbol{P}_{n+1} = W_{,\boldsymbol{F}_{n+1}} \tag{4.19}$$

Eq. (4.17), or, equivalently, (4.19), furnishes the sought stress update. In particular, we verify that W indeed acts as a potential for $\boldsymbol{P}_{n+1}$, as advertised.

The variational statement (4.9) of the constitutive update opens the way for the application of the tools and principles of nonlinear optimization. These tools are particularly useful in the context of multi-surface theories of plasticity. In particular, the efficient determination of active constraints is one of the central problems contemplated in nonlinear optimization, and the methods which have been developed to effect that determination in turn provide a systematic means of determining which internal processes are active, or, equivalently, which yield surfaces are undergoing plastic loading. Some simple models, however, are amenable to an explicit analytical treatment, as demonstrated in the following examples.

EXAMPLE 4.4: Small-strain variational update for an isotropic Mises solid. We begin by considering, by way of illustration, the simple and analytically tractable case of an isotropically hardening Mises solid undergoing small strains. For simplicity, we further assume that the free energy has the additive structure (2.6) and that the elastic response of the material is isotropic. The tensor $\boldsymbol{M}$ which determines the direction of the plastic strain rate $\dot{\boldsymbol{\epsilon}}^{\mathrm{p}}$ follows from the problem:

$$\min_{\boldsymbol{M}} \mu \| \boldsymbol{e}^{\mathrm{e,pre}}_{n+1} - \Delta\epsilon^{\mathrm{p}}\boldsymbol{M} \|^2 \tag{4.20}$$

subject to the constraints (2.21) and (2.22). In (4.20) we have introduced the notation

$$\boldsymbol{e} \equiv \boldsymbol{\epsilon}^{\mathrm{dev}} \tag{4.21}$$

for the deviatoric strain tensor and

$$\boldsymbol{e}^{\mathrm{e,pre}}_{n+1} = \boldsymbol{e}_{n+1} - \boldsymbol{\epsilon}^{\mathrm{p}}_n \tag{4.22}$$

is the predictor deviatoric elastic strain, i.e. the deviatoric elastic strain which would be attained at time t_{n+1} if the solid were to unload elastically. The solution may readily be obtained by recourse to Lagrange multipliers, with the result:

$$\boldsymbol{M} = \sqrt{\frac{3}{2}} \frac{\boldsymbol{e}^{\mathrm{e,pre}}_{n+1}}{\| \boldsymbol{e}^{\mathrm{e,pre}}_{n+1} \|} \tag{4.23}$$

Once optimal direction of plastic flow for the step has been determined, the increment in effective plastic strain follows from the problem:

$$\min_{\Delta\epsilon^{\mathrm{p}}} \mu\|\boldsymbol{e}_{n+1}^{\mathrm{e,pre}} - \Delta\epsilon^{\mathrm{p}}\boldsymbol{M}\|^2 + W^{\mathrm{p}}(\Delta\epsilon^{p}) + \Delta t\,\psi^{*}\left(\frac{\Delta\epsilon^{p}}{\Delta t}\right) \tag{4.24}$$

We note that $\Delta\epsilon^{\mathrm{p}}$ must satisfy the constraint $\Delta\epsilon^{\mathrm{p}} \geqslant 0$ by virtue of (2.51). The value $\Delta\epsilon^{p} = 0$, which corresponds to elastic unloading, defines a non-smooth point of the objective function (4.24). A conventional means of sidestepping this difficulty is to first investigate the solution $\Delta\epsilon^{\mathrm{p}} = 0$, which corresponds to a purely elastic update, or elastic predictor. If the attendant driving force $\sigma - \sigma_{\mathrm{Y}} > 0$ then one must have $\Delta\epsilon^{\mathrm{p}} > 0$ instead, and the solid is loaded plastically. Since the function (4.24) of $\Delta\epsilon^{\mathrm{p}}$ is smooth away from the origin, the case of plastic loading may be solved, e.g. by a local Newton–Raphson iteration.

EXAMPLE 4.5: Variational update for an isotropic Mises solid. Next, we extend into the finite deformation range the treatment given in Example 4.4 to the Mises solid. As in Example 4.4, we consider an isotropically hardening Mises solid possessing a free energy with the additive structure (2.6). The elastic response of the material is further assume to be isotropic. The kinematic tensor $\boldsymbol{A}$ follows from the problem:

$$\min_{\boldsymbol{A}} W^{\mathrm{e}}(\boldsymbol{F}_{n+1}\boldsymbol{F}_{n}^{\mathrm{p}-1}\boldsymbol{A}^{-1}) \tag{4.25}$$

But, by material frame indifference, W^{e} can only depend on $\boldsymbol{F}^{\mathrm{e}}$ through the corresponding elastic right Cauchy–Green deformation tensor $\boldsymbol{C}^{e} = \boldsymbol{F}^{\mathrm{e}\mathrm{T}}\boldsymbol{F}^{\mathrm{e}}$, and (4.25) becomes

$$\min_{\boldsymbol{A}} W^{\mathrm{e}}(\boldsymbol{A}^{-T}\boldsymbol{C}_{n+1}^{\mathrm{e,pre}}\boldsymbol{A}^{-1}) \tag{4.26}$$

where

$$\boldsymbol{C}_{n+1}^{\mathrm{e,pre}} = \boldsymbol{F}_{n}^{\mathrm{p}-\mathrm{T}}\boldsymbol{C}_{n+1}\boldsymbol{F}_{n}^{\mathrm{p}-1} \tag{4.27}$$

is the predictor value of $\boldsymbol{C}_{n+1}^{e}$, i.e. the value that would be obtained if the material underwent elastic unloading. Furthermore, by the assumed elastic isotropy of the material, the incremental plastic deformation tensor $\boldsymbol{A}$ may be assumed to be symmetric without loss of generality. To verify this statement, start from a general $\boldsymbol{A}$ and introduce its polar decomposition $\boldsymbol{A} = \boldsymbol{R}\boldsymbol{U}$, where $\boldsymbol{R} \in \mathrm{SO}(3)$ is a proper rotation and $\boldsymbol{U} = \boldsymbol{U}^{\mathrm{T}}$ is a symmetric tensor. Insertion into (4.26) gives

$$W^{\mathrm{e}}(\boldsymbol{F}_{n+1}\boldsymbol{F}_{n}^{\mathrm{p}-1}\boldsymbol{A}^{-1}) = W^{\mathrm{e}}(\boldsymbol{F}_{n+1}\boldsymbol{F}_{n}^{\mathrm{p}-1}\boldsymbol{U}^{-1}\boldsymbol{R}^{-1}) = W^{\mathrm{e}}(\boldsymbol{F}_{n+1}\boldsymbol{F}_{n}^{\mathrm{p}-1}\boldsymbol{U}^{-1}) \tag{4.28}$$

where the last identity follows from isotropy. It therefore follows that we can identify $\boldsymbol{A} = \boldsymbol{U}$ in calculations. The rotation tensor $\boldsymbol{R}$ remains undetermined in the isotropic case, but this indeterminacy is entirely inconsequential. It also follows that the matrix $\boldsymbol{M}$ may be taken to be symmetric.

As previously stated, the focus of the present example is on models which are amenable to an explicit analytical treatment. One such model consists of assuming an elastic energy density of the form:

$$W^{\mathrm{e}} = f(J^{\mathrm{e}}) + \mu\|\boldsymbol{e}^{\mathrm{e}}\|^2 \tag{4.29}$$

where $J^{\mathrm{e}} = \det(\boldsymbol{F}^{\mathrm{e}})$ is the elastic Jacobian and $\boldsymbol{e}$ obeys a relation of the form (4.21), with

$$\boldsymbol{\epsilon}^{\mathrm{e}} \equiv \frac{1}{2}\log(\boldsymbol{C}^{\mathrm{e}}) \tag{4.30}$$

playing the role of an equivalent elastic strain tensor. We further introduce the predictor

$$\boldsymbol{\epsilon}_{n+1}^{\mathrm{e,pre}} = \frac{1}{2}\log(\boldsymbol{C}_{n+1}^{\mathrm{e,pre}}) \tag{4.31}$$

To make further progress, we introduce the *ansatz* that the symmetric tensors $\boldsymbol{C}_{n+1}^{\mathrm{e,pre}}$ and $\boldsymbol{A}$ commute, i.e. they have the same eigenvectors. Under these conditions, one has the identity

$$\boldsymbol{e}_{n+1}^{\mathrm{e}} = \boldsymbol{e}_{n+1}^{\mathrm{e,pre}} - \Delta\epsilon^{\mathrm{p}}\boldsymbol{M} \tag{4.32}$$

which exactly parallels the small-strain kinematics of Example 4.4. In particular, the plastic flow direction $\boldsymbol{M}$

follows from problem (4.20), the solution of which is, therefore, (4.23). Finally, $\Delta\boldsymbol{\epsilon}^{\mathrm{p}}$ follows from (4.24). The analogy between the finite deformation and small-strain theories of plasticity afforded by the introduction of the exponential and logarithmic mappings has been exploited by Cuitiño and Ortiz [16] to develop a material-independent method of extension of small-strain updates to the finite deformation range.

EXAMPLE 4.6: Variational update for crystals. In applications to crystal plasticity, the variational updates lead, by construction, to an optimal choice of active slip systems. From an optimization perspective, the identification of the active slip systems is equivalent to the determination of the active constraint set, which is the cornerstone of most nonlinear optimization algorithms [9]. Here we have evaluated two alternative approaches, namely, (quasi-)Newton methods and sequential quadratic programming (SQP). The minimization problem of interest can be written in the form:

$$\min_{\gamma^{\beta}_{n+1}} F(\gamma^{\beta}_{n+1}; \boldsymbol{F}_{n+1}, \boldsymbol{F}^{\mathrm{p}}_{n}, \gamma^{\beta}_{n}) \text{ with } \gamma^{\beta}_{n+1} \geqslant \gamma^{\beta}_{n},\ \beta = 1, \ldots, N \tag{4.33}$$

with

$$F(\gamma^{\beta}_{n+1}; \boldsymbol{F}_{n+1}, \boldsymbol{F}^{\mathrm{p}}_{n}, \gamma^{\beta}_{n}) \equiv W^{\mathrm{e}}(\boldsymbol{F}\boldsymbol{F}^{\mathrm{p}\,-1}_{n}\boldsymbol{A}^{-1}(\gamma^{\beta}_{n+1})) + W^{\mathrm{p}}(\gamma^{\beta}_{n+1}) + \Delta t\, \psi^{*}\left(\frac{\gamma^{\beta}_{n+1} - \gamma^{\beta}_{n}}{\Delta t}, \gamma_{n+\alpha}\right) \tag{4.34}$$

Conveniently, in the case of single-crystal plasticity the only unknowns are the updated slip strains, and no additional kinematic parameters need be considered. In particular, the appropriate flow-rule tensor is

$$\boldsymbol{A} = \exp(\boldsymbol{M}) = \exp\left\{\sum_{\beta=1}^{N} \Delta\gamma^{\beta}\, \boldsymbol{s}^{\beta} \otimes \boldsymbol{m}^{\beta}\right\} \tag{4.35}$$

Algorithm 1
Projected Newton method

(i) Initialize the set of active constraints $\mathscr{L}$
$\gamma^{\alpha}_{(0)} = \gamma^{\alpha}_{n},\ \alpha = 1, \ldots, N$

(ii) $\Delta\gamma^{\alpha} = -(F_{,\gamma\gamma})^{-1}_{\alpha\beta} F_{,\gamma\beta},\ \alpha \notin \mathscr{L}$
$\Delta\gamma^{\alpha} = 0,\ \alpha \in \mathscr{L}$

(iii) If $\|\Delta\boldsymbol{\gamma}\| < \epsilon$ find $\delta: F_{,\gamma\delta} = \min_{\alpha\in\mathscr{L}}(F_{,\gamma\alpha})$
If $F_{,\gamma\delta} < 0$
remove δ from $\mathscr{L}$, go to (ii)
else
go to (v)

(iv) Find $\bar{\lambda} = \min_{\alpha\notin\mathscr{L}}\{\lambda > 0: \gamma^{\alpha}_{(k)} + \lambda\ \Delta\gamma^{\alpha} = \gamma^{\alpha}_{n}\}$ (corresponding index $= \delta$)
If $\Sigma_{\alpha}\ \Delta\gamma^{\alpha}\ F_{,\gamma\alpha}(\boldsymbol{\gamma}_{(k)} + \bar{\lambda}\ \Delta\boldsymbol{\gamma}) \leqslant 0$
add δ to $\mathscr{L}$
$\gamma^{\alpha}_{(k+1)} = \gamma^{\alpha}_{(k)} + \bar{\lambda}\Delta\gamma^{\alpha},\ \alpha \notin \mathscr{L}$
else
find optimal λ^{*} along $\Delta\gamma^{\alpha}$
$\gamma^{\alpha}_{(k+1)} = \gamma^{\alpha}_{(k)} + \lambda^{*}\ \Delta\gamma^{\alpha},\ \alpha \notin \mathscr{L}$
go to (ii)

(v) $\gamma^{\alpha}_{n+1} = \gamma^{\alpha}_{(k)},\ \alpha = 1, \ldots, N$

The projected Newton algorithm is outlined as Algorithm 1. The line-search step notwithstanding, this algorithm is similar in spirit to one previously proposed by Cuitiño and Ortiz [17] for the identification of the active slip systems. In both approaches, the active-set strategy consists of releasing the constraints one by one

based on the value of their Lagrangian multipliers, which amounts to adding the slip system for which the yield criterion is most violated. However, a notable difference is that here we release a constraint only after a local minimum is reached in the projected space. This avoids zigzagging, a common problem in very constrained problems such as considered here.

Algorithm 2
Sequential Quadratic Programming

(i) Initialize the set of active constraints $\mathscr{L}$
$\gamma^{\alpha}_{(0)} = \gamma^{\alpha}_{n}$, $\alpha = 1, \ldots, N$

(ii) Solve the quadratic problem

$$\min Q(\Delta\boldsymbol{\gamma}) \equiv \Delta\boldsymbol{\gamma}^{\mathrm{T}} F_{,\boldsymbol{\gamma}}(\boldsymbol{\gamma}_{(k)}) + \frac{1}{2}\Delta\boldsymbol{\gamma}^{T} F_{,\boldsymbol{\gamma}\boldsymbol{\gamma}}(\boldsymbol{\gamma}_{(k)})\,\Delta\boldsymbol{\gamma}$$

with $\gamma^{\alpha}_{(k)} + \Delta\gamma^{\alpha} \geqslant \gamma^{\alpha}_{n}$, $\alpha = 1, \ldots, N$

(iii) If $\|\Delta\boldsymbol{\gamma}\| < \epsilon$ go to (v)

(iv) Find $\bar{\lambda} = \min_{\alpha \notin \mathscr{L}}\{\lambda > 0 : \gamma^{\alpha}_{(k)} + \lambda\,\Delta\gamma^{\alpha} = \gamma^{\alpha}_{n}\}$ (corresponding index $= \delta$)
If $\Sigma_{\alpha}\,\Delta\gamma^{\alpha} F_{,\gamma^{\alpha}}(\boldsymbol{\gamma}_{(k)} + \bar{\lambda}\,\Delta\boldsymbol{\gamma}) \leqslant 0$
add δ to $\mathscr{L}$
$\gamma^{\alpha}_{(k+1)} = \gamma^{\alpha}_{(k)} + \bar{\lambda}\,\Delta\gamma^{\alpha}$, $\alpha \notin \mathscr{L}$
else
find optimal λ^{*} along $\Delta\gamma^{\alpha}$
$\gamma^{\alpha}_{(k+1)} = \gamma^{\alpha}_{(k)} + \lambda^{*}\,\Delta\gamma^{\alpha}$, $\alpha \notin \mathscr{L}$
go to (ii)

(v) $\gamma^{\alpha}_{n+1} = \gamma^{\alpha}_{(k)}$, $\alpha = 1, \ldots, N$

The SQP algorithm is listed as Algorithm 2. The algorithm replaces the nonlinear problem by a sequence of quadratic problems, which can be solved efficiently by a constrained conjugate gradient method. It should be noted that constraint removal is treated as a part of the quadratic programming step, with the same active-set strategy as in the projected Newton method described earlier. One advantage in using the SQP method is that most of the work in determining the active set of constraints, or slip systems, is accomplished on the basis of a quadratic function. This stabilizes the iterative process and also helps to avoid zigzagging between the constraints. The iterations are mostly performed within the quadratic problem, thus reducing the number of evaluations of the Hessian matrix ($F_{,\gamma^{\alpha}_{n+1}\gamma^{\beta}_{n+1}}$).

For both algorithms, direct evaluation of the Hessian matrix may be replaced by a quasi-Newton update. This may help to maintain convergence in cases in which the update is applied to a non-convex hardening model, such as the latent hardening model described above. However, the exact Hessian is required in order to compute the consistent tangent moduli.

It bears emphasis that the theoretical and practical insights revealed by nonlinear optimization theory apply generally to all multi-surface plasticity models and are not restricted to crystal plasticity.

The tangent moduli corresponding to the variational updates follow from a direct linearization of (4.19), with the result:

$$\frac{\partial \boldsymbol{P}_{n+1}}{\partial \boldsymbol{F}_{n+1}} = W_{,\boldsymbol{F}_{n+1}\boldsymbol{F}_{n+1}} + W_{,\boldsymbol{F}_{n+1}\boldsymbol{Q}_{n+1}} \cdot \frac{\partial \boldsymbol{Q}_{n+1}}{\partial \boldsymbol{F}_{n+1}} + W_{,\boldsymbol{F}_{n+1}\boldsymbol{K}} \cdot \frac{\partial \boldsymbol{K}}{\partial \boldsymbol{F}_{n+1}} \tag{4.36}$$

The sensitivities to $\boldsymbol{Q}_{n+1}$ and $\boldsymbol{K}_{n+1}$ derive from the stationarity condition of W, which gives

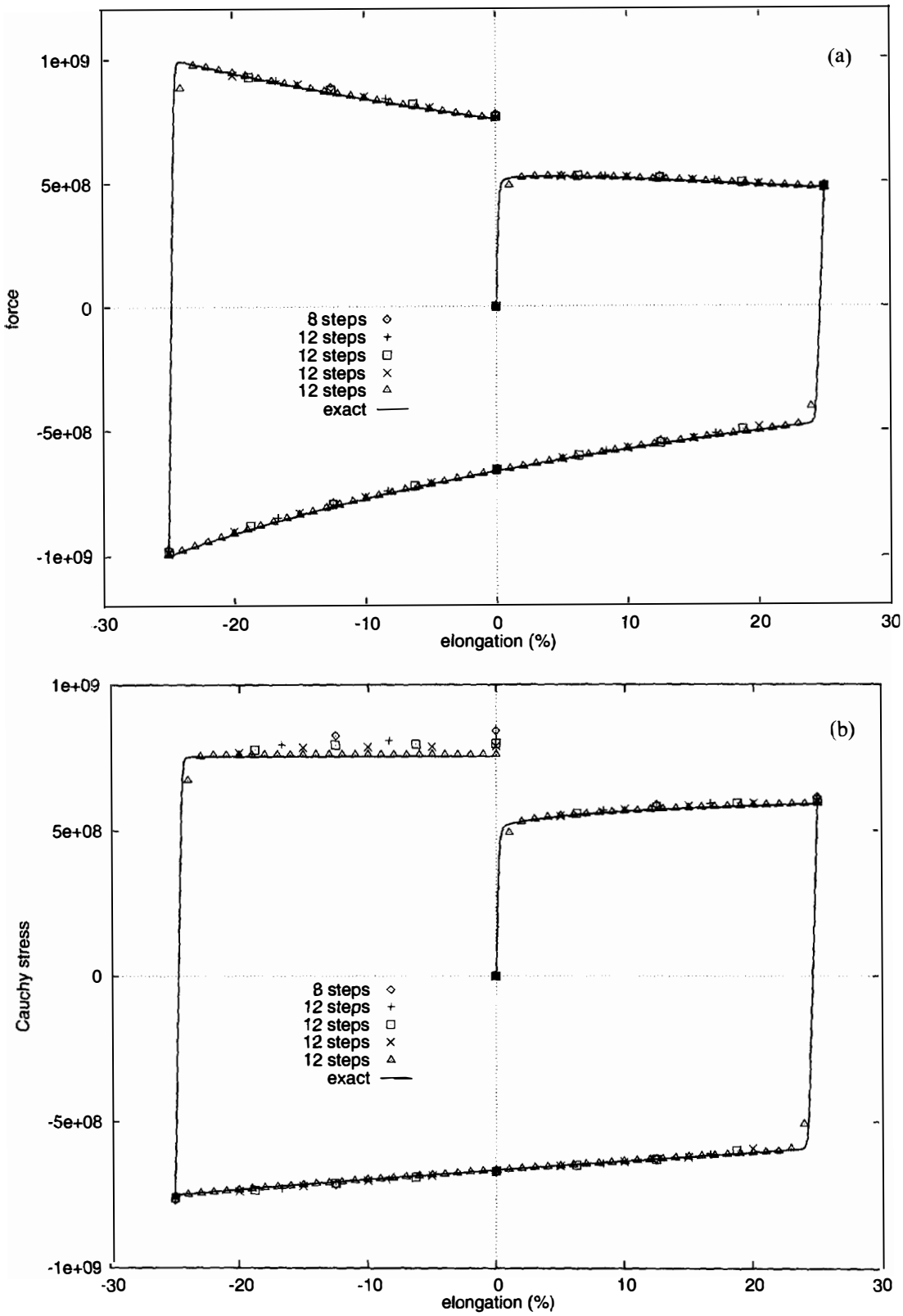

Fig. 1. Isotropic Mises solid under cyclic loading. (a) Axial force, (b) axial Cauchy stress, (c) equivalent plastic strain, (d) cross-section area

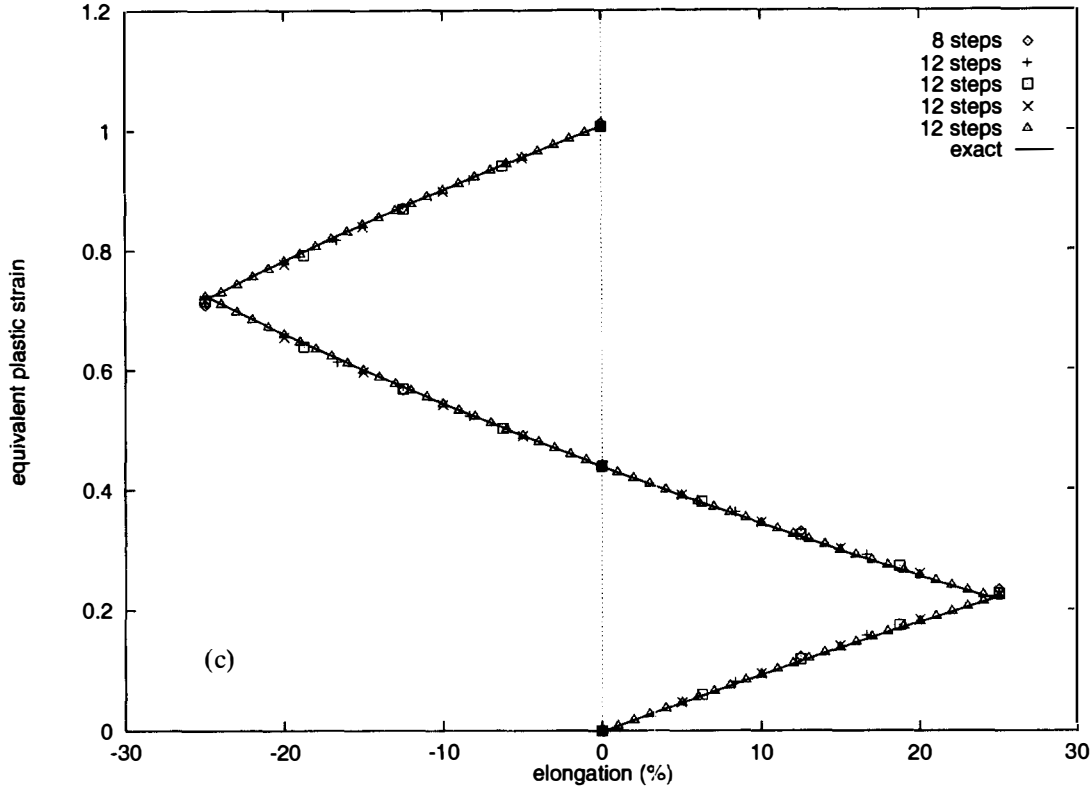

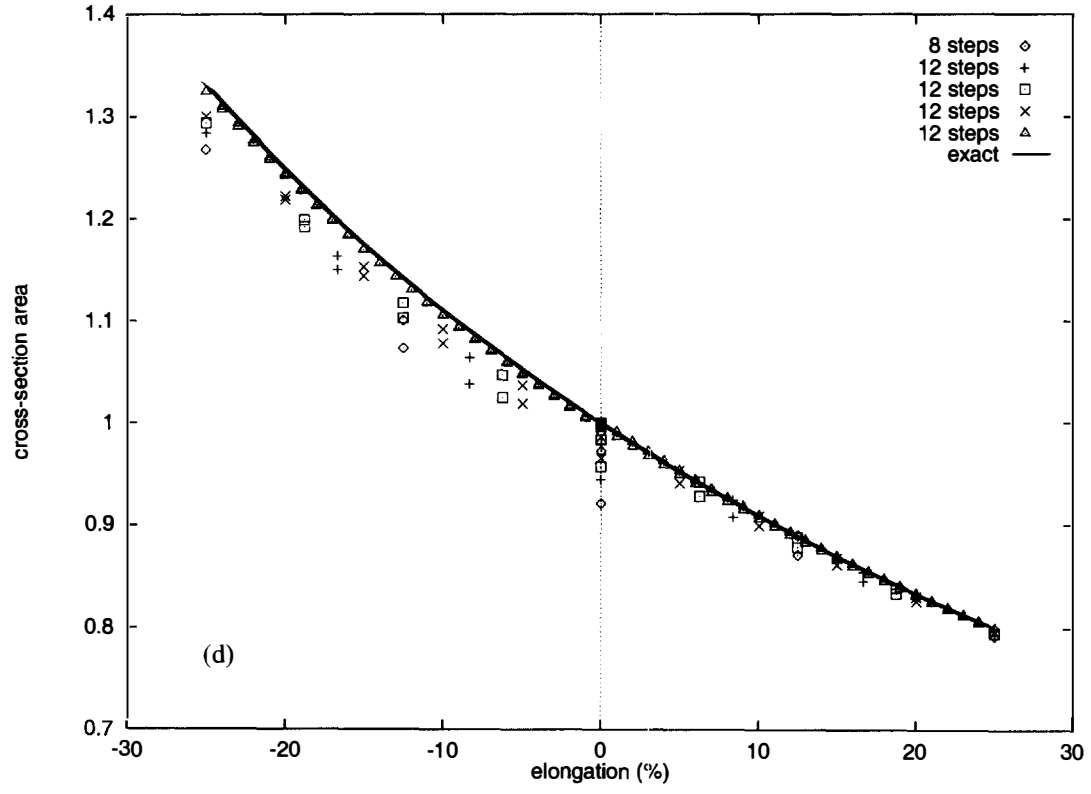

Fig. 1. Continued.

$$W_{,\boldsymbol{Q}_{n+1}\boldsymbol{F}_{n+1}} + W_{,\boldsymbol{Q}_{n+1}\boldsymbol{Q}_{n+1}} \cdot \frac{\partial \boldsymbol{Q}_{n+1}}{\partial \boldsymbol{F}_{n+1}} + W_{,\boldsymbol{Q}_{n+1}\boldsymbol{K}} \cdot \frac{\partial \boldsymbol{K}}{\partial \boldsymbol{F}_{n+1}} = 0 \tag{4.37}$$

$$W_{,\boldsymbol{K}\boldsymbol{F}_{n+1}} + W_{,\boldsymbol{K}\boldsymbol{Q}_{n+1}} \cdot \frac{\partial \boldsymbol{Q}_{n+1}}{\partial \boldsymbol{F}_{n+1}} + W_{,\boldsymbol{K}\boldsymbol{K}} \cdot \frac{\partial \boldsymbol{K}}{\partial \boldsymbol{F}_{n+1}} = 0 \tag{4.38}$$

Eqs. (4.37) and (4.38) form a linear system of equations, the solution of which may be inserted in (4.36) to yield

$$\frac{\partial \boldsymbol{P}_{n+1}}{\partial \boldsymbol{F}_{n+1}} = W_{,\boldsymbol{F}_{n+1}\boldsymbol{F}_{n+1}} - \{W_{,\boldsymbol{F}_{n+1}\boldsymbol{Q}_{n+1}} W_{,\boldsymbol{F}_{n+1}\boldsymbol{K}}\} \cdot \begin{pmatrix} W_{,\boldsymbol{Q}_{n+1}\boldsymbol{Q}_{n+1}} & W_{,\boldsymbol{Q}_{n+1}\boldsymbol{K}} \\ W_{,\boldsymbol{K}\boldsymbol{Q}_{n+1}} & W_{,\boldsymbol{K}\boldsymbol{K}} \end{pmatrix}^{-1} \cdot \begin{Bmatrix} W_{,\boldsymbol{Q}_{n+1}\boldsymbol{F}_{n+1}} \\ W_{,\boldsymbol{K}\boldsymbol{F}_{n+1}} \end{Bmatrix} \tag{4.39}$$

In writing this expression, we have assumed that the linear system deriving from the stationarity conditions is nonsingular.

It should be carefully noted that the function W is incremental in nature and depends on the initial conditions $\{\boldsymbol{F}_n, \boldsymbol{F}^{\mathrm{p}}_n, \boldsymbol{Q}_n\}$ for the time step. This in turn allows for hysteretic behavior, as required. A distinct advantage of stress updates possessing a potential structure, such as just formulated, is that the tangent moduli $\partial \boldsymbol{P}_{n+1}/\partial \boldsymbol{F}_{n+1}$ are symmetric, which in turn results in symmetric tangent stiffness matrices upon finite element discretization. The existence of a symmetric and coercive Dirichlet form, leading to error estimates in the energy norm, is directly related to the convexity properties of the incremental strain energy density $W(\boldsymbol{F}_{n+1}; \boldsymbol{F}_n, \boldsymbol{Q}_n)$, [58].

5. Numerical examples

In this section we investigate the convergence properties of the variational updates just derived by way of direct numerical testing. We also illustrate the robustness conferred to the updates by the optimization procedure as regards the selection of active slip systems in single crystals. This robustness is effectively tested in cases in which the crystal is loaded in uniaxial tension in a direction which is close to a high-symmetry axis. Under these conditions, the determination of the pattern of slip activity is a nontrivial proposition, as the outcome depends very sensitively on small misalignments of the loading direction.

5.1. Isotropic mises solid

We begin by considering the case of an isotropic Mises solid subjected to uniaxial cyclic loading. The elastic energy density has the form (4.29) with

$$f(J^{\mathrm{e}}) = \frac{1}{2}\left(\lambda + \frac{2\mu}{3}\right)(\log(J^{\mathrm{e}}))^2 \tag{5.1}$$

while the plastic energy density has the form (2.8), corresponding to power-law hardening. In order to speed-up the calculations, the deviatoric part of the logarithmic strain (4.31) is approximated to first order. The rate sensitivity of the solid is governed by a dual potential of the power-law form (2.50). The material parameters employed in the calculations are collected in Table 1.

A uniaxial cyclic loading test is simulated using a single 8-node brick element loaded along its z-axis. One symmetric tension-compression cycle is applied to the element up to a maximum extension of 25% at a nominal strain rate of $\pm 100\%/\mathrm{s}$. The convergence of the numerical solutions with decreasing time step is illustrated in Fig. 1. The reference solution, labeled as exact in the plots, is obtained in 1000 steps and is ostensibly indistinguishable from the exact solution. Fig. 1(a–d) display the computed forces, axial Cauchy stress,

Table 1
Material parameters for isotropic Mises solid

λ	μ	Y_0	Q_0	n	$\dot{Q}_0$	m
125 GPa	84 GPa	250 MPa	1	2	1	2

equivalent plastic strain, and cross-section reduction, respectively. The strong convergence of the numerical solution and the excellent accuracy obtained with relatively large steps is evident from these figures.

Convergence plots are shown in Fig. 2(a) and (b) for a range of hardening and rate-sensitivity exponents, respectively. Error are measured in terms of the axial Cauchy stress at the end of the cycle. The values of the hardening exponent considered in the calculations range from linear hardening, $n = 1$, to negligible hardening or ideal plasticity, $n = 10^6$. Likewise, the rate-sensitivity exponent is allowed to vary from $m = 1$, or linear rate-sensitivity to nearly rate-insensitive or inviscid behavior, $m = 10^6$. It is noteworthy that the updates remain well conditioned even for exceedingly large values of the exponents m and n. Variations of the parameters Q_0 and $\dot{Q}_0$ simply result in a re-normalization of the strain and strain rate, respectively. In all cases, the computed rate of convergence is linear and the errors are remarkably insensitive to variations in the material parameters. In particular, the accuracy of the solution appears to be essentially independent of the hardening exponent n, Fig. 2(a), and is only moderately dependent on the rate-sensitivity exponent m, Fig. 2(b).

The numerical tests just described, and other similar tests, attest to the strong convergence of the method. Unfortunately, analytical tools suited to the assessment of the convergence properties of finite-deformation constitutive updates are not as yet in existence. The situation is compounded by the fact, pointed out by Ball [4], that the strain energy density of a finitely deforming solid W must necessarily be non-convex. This effectively precludes the application of the conventional tools of convex analysis to the analysis of general constitutive updates.

5.2. Single crystal

Our next test concerns the performance of the variational updates in the context of multi-surface plasticity. In particular, we consider a copper single crystal subjected to uniaxial tension. For simplicity, the elastic energy density is taken to be of the form:

$$W^{\mathrm{e}} = \frac{1}{2}\, \boldsymbol{E}^{\mathrm{e}} : \mathscr{C} : \boldsymbol{E}^{\mathrm{e}} \tag{5.2}$$

where $\boldsymbol{E}^{\mathrm{e}} = (\boldsymbol{C}^{\mathrm{e}} - \boldsymbol{I})/2$ is the elastic Green–Lagrange strain tensor, and $\mathscr{C}$ is an anisotropic (cubic) elasticity tensor parameterized by the three independent moduli C_{11}, C_{12} and C_{44}. For metallic single crystals, the particular form of the elastic strain energy is often of little consequence as the elastic strains are in most cases small. An exception is furnished by shock-loaded crystals, in which case the appropriate choice of equation of state is of critical importance.

A simple example of a latent-hardening model possessing the requisite potential structure has been given in Section 2, Eq. (2.42), for purposes of illustration. Unfortunately, few of the commonly used models of single-crystal hardening, which for the most part are based on the direct formulation of a hardening matrix, derive from a potential. In order to be able to bring these models into conformity with the variational framework envisioned here, we simply treat the hardening matrix explicitly by sampling it at the beginning of the time step. Provided that the hardening matrix is symmetric, this is tantamount to a step-by-step quadratic approximation for the stored energy W^{p}, namely,

$$W^{\mathrm{p}}(\boldsymbol{\gamma}_{n+1}) = W^{\mathrm{p}}_n + \sum_{\alpha} \left(g^{\alpha}_n (\gamma^{\alpha}_{n+1} - \gamma^{\alpha}_n) + \frac{1}{2} (\gamma^{\alpha}_{n+1} - \gamma^{\alpha}_n) \sum_{\beta} h^{\alpha\beta}_n (\gamma^{\beta}_{n+1} - \gamma^{\beta}_n) \right) \tag{5.3}$$

where g^{α}_n is the critical resolved shear stress for system α at the beginning of the step. In the calculations reported here, the hardening matrix $h^{\alpha\beta}$ is taken to be diagonal and of the form [17]:

$$h^{\alpha\alpha} = h^{\alpha}_c \left(\frac{g^{\alpha}}{\tau^{\alpha}_c} \right)^3 \left\{ \cosh \left[\left(\frac{\tau^{\alpha}_c}{g^{\alpha}} \right)^2 \right] - 1 \right\}, \quad \text{no sum} \tag{5.4}$$

where

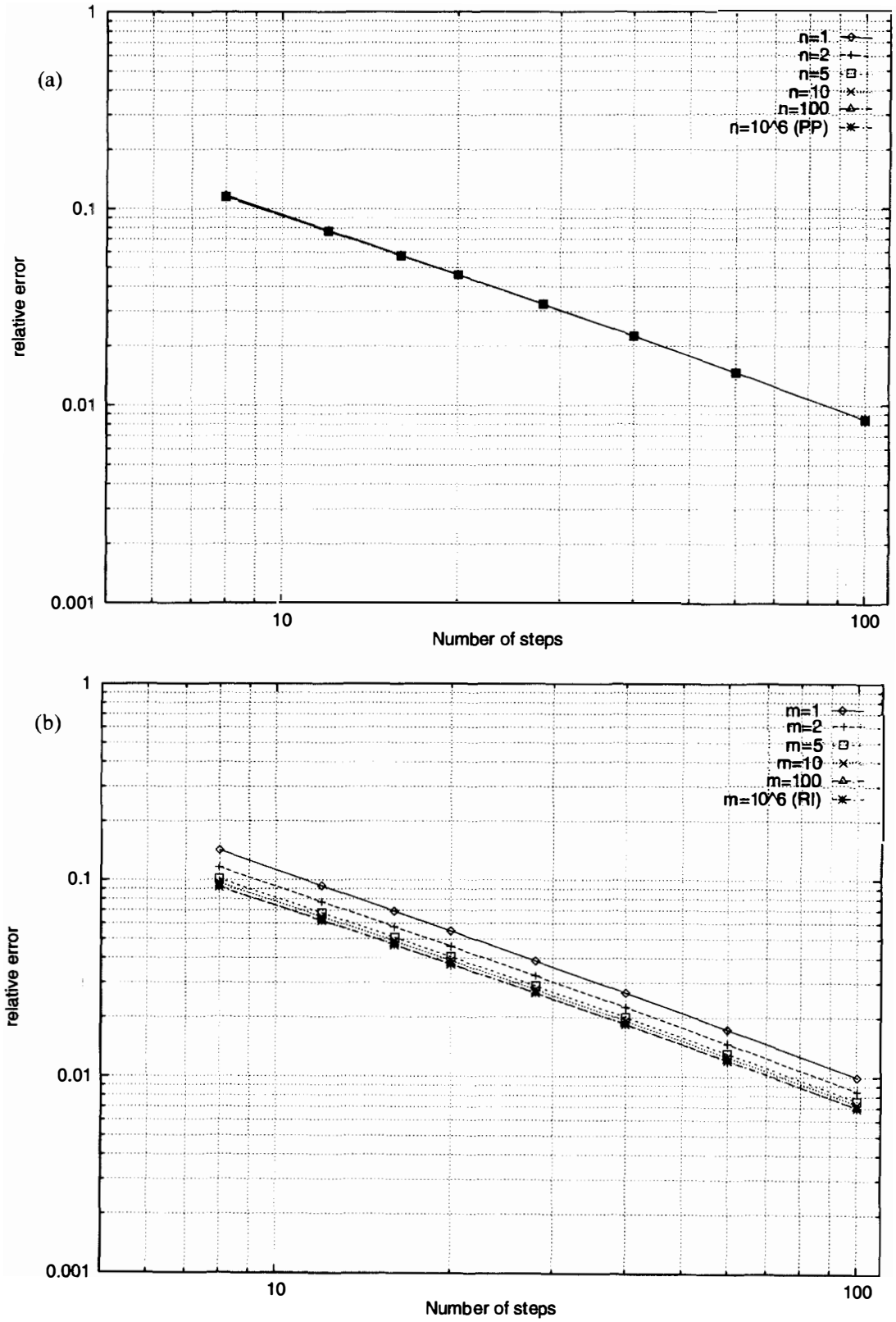

Fig. 2. Isotropic Mises solid: convergence plots. (a) Fixed rate-dependency ($m = 2$), varying hardening (exponent n); (b) fixed hardening ($n = 2$), varying rate-dependency (exponent m).

$$h_c^\alpha = \frac{\tau_c^\alpha}{\gamma_c^\alpha}, \qquad \tau_c^\alpha \equiv \alpha\mu b\sqrt{\pi n^\alpha}, \qquad \gamma_c^\alpha \equiv \frac{b\rho^\alpha}{2\sqrt{n^\alpha}} \tag{5.5}$$

define a characteristic plastic modulus, critical resolved shear stress and slip strain for slip system α, respectively. In addition, ρ^α is the corresponding dislocation density, and

$$n^\alpha = \sum_\beta a^{\alpha\beta}\rho^\beta \tag{5.6}$$

is the point-obstacle density due to forest dislocations, respectively. The coefficients $a^{\alpha\beta}$ in (5.6) describe the interactions between the different systems. For f.c.c. crystals, these interactions have been classified by Franciosi and Zaoui [22] in four categories in accordance with their strength, with corresponding coefficients a_0, a_1, a_2, a_3 ($a_0 \leq a_1 \leq a_2 \leq a_3$). Finally, dislocation multiplication may simply be modeled through a relation of the form:

$$\rho^\alpha = \rho_{\text{sat}}\left[1 - \left(1 - \frac{\rho_0}{\rho_{\text{sat}}}\right)\exp - \gamma^*/\gamma_{\text{sat}}\right] \tag{5.7}$$

where ρ_0 is the initial dislocation density, ρ_{sat} is the saturation density and γ_{sat} is a characteristic slip strain for saturation. As in the preceding example, the rate sensitivity is governed by a dual potential of the form (2.50). The material parameters used in calculations are collected in Table 2.

The orientation of the crystal relative to the loading direction is of major importance, as it determines the resolved shear stresses on the different slip systems. We begin by considering the case of a tensile axis oriented in the [001] direction. As a consequence of the high symmetry of this orientation—and despite the apparent simplicity of the problem—the determination of the active slip-system set becomes numerically challenging. Data from an actual SQP iteration are shown in Table 3. As may be seen, only two SQP steps are required for convergence, and most of the work is accomplished in the first iteration, which comprises ten CG sub-iterations. These sub-iterations are mostly required for the determination of the active systems. As expected from the resolved shear stress distribution, the slip activity consists of eight equally active systems out of a maximum twenty-four available slip systems (accounting for positive and negative slip directions), Fig. 3(a). In all figures, we have adopted Schmid and Boas' nomenclature [62] to designate the slip systems of a f.c.c. crystal. Due to the multi-slip character of the deformation, the attendant stress–strain curve is predominantly parabolic, Fig. 4.

The response of the [001] crystal is very sensitive to small misalignments of the loading axis. This sensitivity is illustrated in Fig. 3(b), which shows the slip activity resulting from a 1% misalignment. As may be seen, the slip activity involves fewer active systems than in the case of a perfect [001] orientation and, owing to the

Table 2
Material parameters for a copper single crystal

C_{11}	C_{12}	C_{44}	$\dot{\gamma}_0$	m	τ_0	ρ_0	ρ_{sat}	γ_{sat}
168.4 GPa	121.4 GPa	75.4 GPa	1	100	1 MPa	$1.e^{12}$ m^{-2}	$1.e^{15}$ m^{-2}	0.5%
a_0	a_1	a_2	a_3	α	b			
$1.0e^{-4}$	$5.7a_0$	$10.2a_0$	$16.6a_0$	0.3	$2.56e^{-10}$ m			

Table 3
SQP algorithm for single crystal plasticity

SQP	W	Nit CG
0	2.115538E+06	10
1	1.738655E+06	1
2	1.738655E+06	0

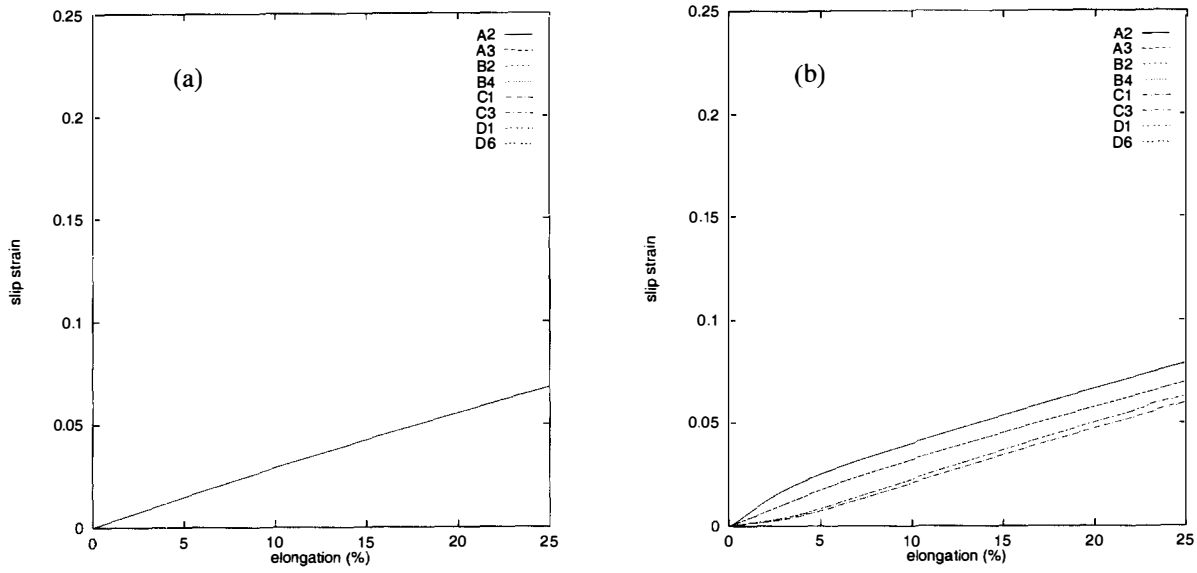

Fig. 3. Slip strain curves of active systems for loading along [001]. (a) Perfect alignment; (b) with alignment defect.

attendant reduction in latent hardening, the stress levels are correspondingly lower, Fig. 4. This sensitivity to the orientation of the crystal, which in itself is a manifestation of the latent hardening, may render the optimization problem very ill-conditioned. It should be noted, however, that this poor conditioning reflects an intrinsic attribute of the material behavior, and is not in any way introduced by the update.

The critical importance of latent hardening in shaping the response of single crystals is clearly illustrated by our next example, which concerns a crystal loaded in the [112] direction. When the loading axis is perfectly aligned, the systems which are activated are principally A3 and D1, which are equally active, and to a lesser extent A6 and D6, which are also equi-active, Fig. 5(a). However, when a small misalignment is introduced, a

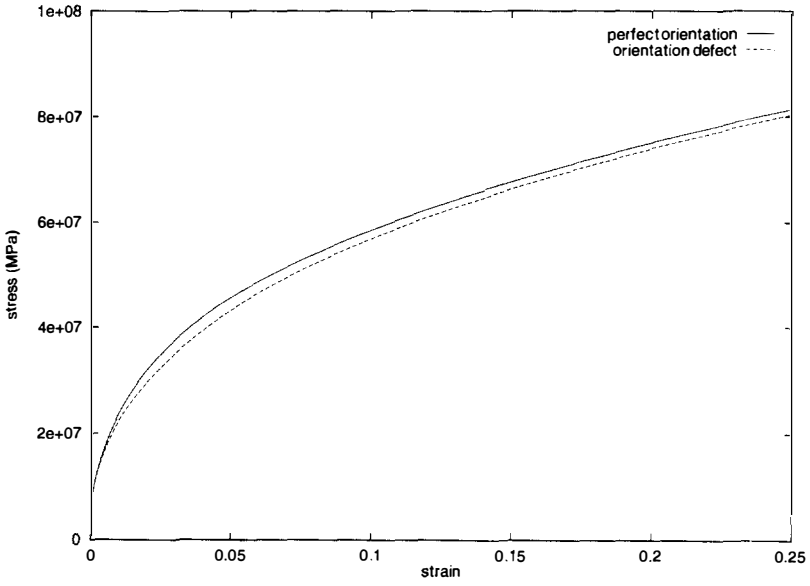

Fig. 4. Global axial stress–strain curves for loading along [001].

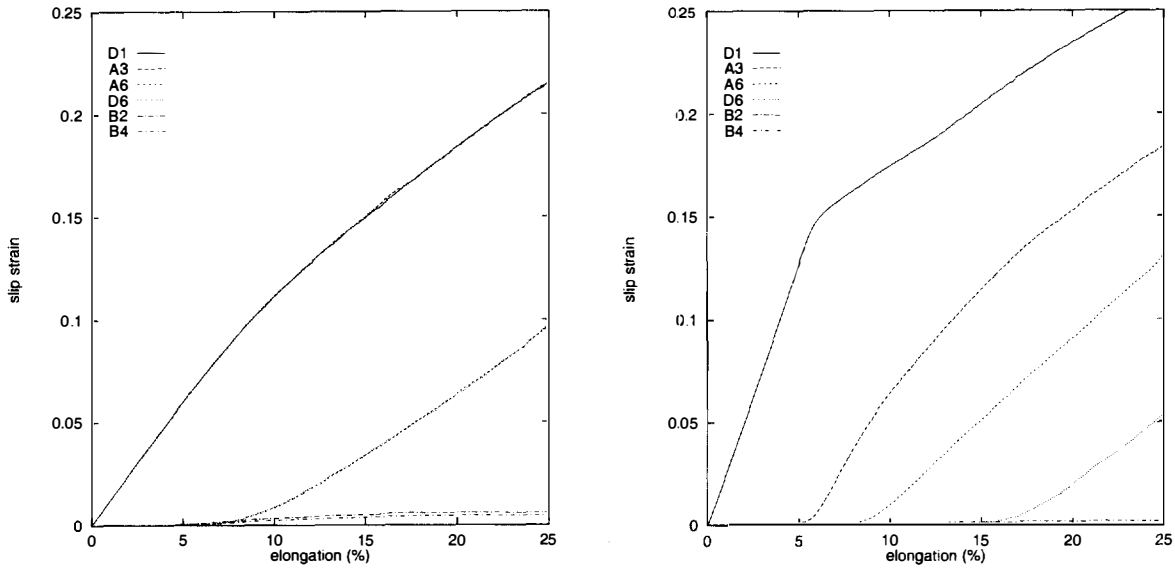

Fig. 5. Slip strain curves of active systems for loading along [112]. (a) Perfect alignment; (b) with alignment defect.

symmetry breaking occurs and the activities of the systems in each pair of nominally equi-active systems becomes different. For instance, the particular defect introduced in our calculations causes the D1 system to be more loaded than the A3 system. In consequence, D1 yields first and, by virtue of latent hardening, greatly hardens the remaining systems. The onset of slip on A3 is thus delayed. This stage of the stress–strain curve is characterized by single slip, or easy glide, and, therefore, corresponds to the experimentally observed stage I of hardening of f.c.c. crystals. Eventually A3 is activated, Fig. 5(b), and this activity rapidly hardens the system D1, which manifests itself as an upturn in the stress–strain curve, Fig. 6. This upturn is in keeping with the experimentally observed stage II of hardening of f.c.c. crystals. As in the [001] crystal, the ability of the update to effectively discern these fine nuances of the slip activity is noteworthy.

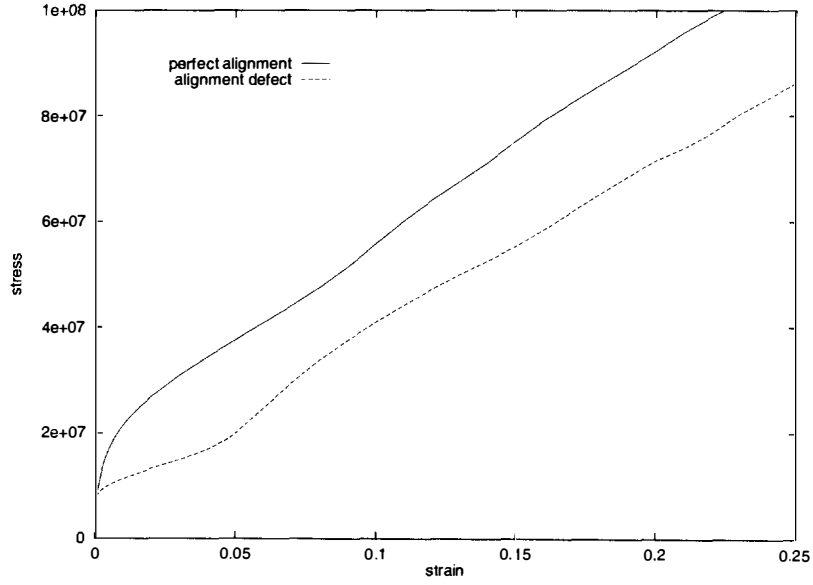

Fig. 6. Global axial stress–strain curves for loading along [112].

6. Summary and conclusions

We have presented a class of constitutive updates for general viscoplastic solids including such aspects of material behavior as finite elastic and plastic deformations, non-Newtonian viscosity, rate-sensitivity and arbitrary flow and hardening rules. The constitutive framework adopted here is based on a conventional internal-variable formulation of continuum thermodynamics [33,34], augmented by the consideration of non-Newtonian viscosity and such non-holonomic internal constraints as are required to describe the plastic flow rule.

The cornerstone of the variational updates proposed here is a time-discretized variational statement of the constitutive relations. We have shown that the minimization of a quasi-thermodynamic function which combines the free energy of the solid, the conjugate inelastic potential for the kinetic equations and the viscous potential, jointly returns the updated value of the internal variables and the effective plastic flow direction, or flow rule, over the time step. In addition, we have shown that the minimum of the quasi-thermodynamic function thus obtained acts as a potential for the stress–strain relations, thus ensuring the variational character of the update. This in turn confers the incremental boundary value problem a variational structure which may be exploited in order to derive error estimates and mesh-adaption strategies [58].

The core of the variational updates is, therefore, a nonlinear optimization problem for the updated internal variables and such kinematic parameters as determine the plastic flow direction. In the case of multi-surface plasticity the determination of the active constraints, or, equivalently, the active systems, becomes the central concern. We have evaluated two alternative approaches, namely, (quasi-)Newton methods and sequential quadratic programming (SQP). In both cases, the ability of the updates to resolve the complex patterns of slip activity which may arise in single crystals in consequence of latent hardening is particularly noteworthy.

The convergence properties of the variational updates have been investigated by way of numerical testing. In all cases considered, the updates exhibit good accuracy at large time steps and strong linear convergence. In particular, the accuracy of the update is relatively insensitive to parameters such as the hardening and rate-sensitivity exponents.

Acknowledgements

The support of the DOE through Caltech's ASCI Center for the Simulation of the Dynamic Response of Materials is gratefully acknowledged.

References

[1] F. Armero and J.C. Simo, A new unconditionally stable fractional step method for non-linear coupled thermomechanical problems, Int. J. Numer. Methods Engrg. 35 (1992) 737–766.

[2] F. Armero and J.C. Simo, A priori stability estimates and unconditionally stable product formula algorithms for nonlinear coupled thermoplasticity, Int. J. Plasticity 9 (1993) 749–782.

[3] R.J. Asaro and J.R. Rice, Strain localization in ductile single crystals, J. Mech. Phys. Solids 25 (1977) 309.

[4] J.M. Ball, Constitutive inequalities and existence theorems in nonlinear elastostatics, in: R.J. Knops, ed., Nonlinear Analysis and Mechanics: Heriot-Watt Symposium, Volume I (Pitman Publishing Ltd., 1977) 187–241.

[5] J.M. Ball and R.D. James, Fine phase mixtures as minimizers of energy, Arch. Rat. Mech. Anal. 100 (1987) 13–52.

[6] J.L. Bassani and T.Y. Wu, Latent hardening in single crystals. 1. Theory and experiments, Proc. Roy. Soc. Lond., A 435 (1991) 1–19.

[7] J.L. Bassani and T.Y. Wu, Latent hardening in single crystals. 2. Analytical characterization and predictions, Proc. Roy. Soc. Lond., A 435 (1991) 21–41.

[8] T. Belytschko and M. Tabbara, *H*-Adaptive finite element methods for dynamic problems, with emphasis on localization, Int. J. Numer. Methods Engrg. 36 (1993) 4245–4265.

[9] D.P. Bertsekas, Nonlinear Programming (Athena Scientific, Belmont, MA, 1995).

[10] G.T. Camacho and M. Ortiz, Computational modelling of impact damage in brittle materials, Int. J. Solids Struct. 33 (20–22) (1996) 2899–2938.

[11] G.T. Camacho and M. Ortiz, Adaptive Lagrangian modelling of ballistic penetration of metallic targets, Comput. Methods Appl. Mech. Engrg. 142 (1997) 269–301.

[12] P. Carter and J.B. Martin, Work bounding functions for plastic materials, J. Appl. Mech. 98 (1976) 434–438.

[13] M. Chipot and D. Kinderlehrer, Equilibrium configurations of crystals, Arch. Rati. Mech. Anal. 103 (1988) 237–277.

[14] P.G. Ciarlet, Numerical analysis of the finite element method, Les Presses de L'Université de Montréal, Québec, Canada, 1976.
[15] C. Comi and U. Perego, A unified approach for variationally consistent finite elements in elastoplasticity, Comput. Methods Appl. Mech. Engrg. 121 (1995) 323–344.
[16] A.M. Cuitiño and M. Ortiz, A material-independent method for extending stress update algorithms from small-strain plasticity to finite plasticity with multiplicative kinematics, Engrg. Comput. 9 (1992) 437–451.
[17] A.M. Cuitiño and M. Ortiz, Computational modelling of single crystals, Modell. Simul. Mater. Sci. Engrg. 1 (1992) 255–263.
[18] A.M. Cuitiño and M. Ortiz, Constitutive modeling of $L1_2$ intermetallic crystals, Mater. Sci. Engrg. A 170 (1993) 111–123.
[19] A.L. Eterovic and K.J. Bathe, A hyperelastic-based large strain elasto-plastic constitutive formulation with combined isotropic-kinematic hardening using the logarithmic stress and strain measures, Int. J. Numer. Methods Engrg. 30 (1990) 1099–1114.
[20] R.A. Eve, B.D. Reddy and R.T. Rockafellar, An internal variable theory of elastoplasticity based on the maximum plastic work inequality, Quart. Appl. Math. 48(1) (1990) 59–83.
[21] P. Franciosi, M. Berveiller and A. Zaoui, Latent hardening in copper and aluminium single crystals, Acta Metall. 28 (1980) 273–283.
[22] P. Franciosi and A. Zaoui, Multislip in F.C.C. crystals: A theoretical approach compared with experimental data, Acta Metall. 30 (1982) 1627.
[23] W. Han, S. Jensen and B.D. Reddy, Numerical approximations of problems in plasticity: error analysis and solution algorithms, Numer. Linear Algebra Applic. 4 (1997) 191–204.
[24] W. Han, B.D. Reddy and G.C. Schroeder, Qualitative and numerical analysis of quasi-static problems in elastoplasticity, SIAM J. Numer. Anal. 34 (1997) 143–177.
[25] K.S. Havner, On the mechanics of crystalline solids, J. Mech. Phys. Solids 21 (1973) 383.
[26] R. Hill and J.R. Rice, Constitutive analysis of elastic-plastic crystals at arbitary strains, J. Mech. Phys. Solids 20 (1972) 401.
[27] T.J.R. Hughes, Analysis of transient algorithms with particular reference to stability behavior, in: T. Belytschko and T.J.R. Hughes, eds., Computational Methods for Transient Analysis, (North-Holland, 1983) 67–155.
[28] U.F. Kocks, Latent hardening and secondary slip in aluminum and silver, Trans. Metall. Soc. AIME 230 (1964) 1160.
[29] U.F. Kocks, A statistical theory of flow stress and work-hardening, Philos. Magazine 13 (1966) 541.
[30] E.H. Lee, Elastic-plastic deformation at finite strains, J. Appl. Mech. 36 (1969) 1.
[31] N.S. Lee and K.J. Bathe, Error indicators and adaptive remeshing in large deformation finite element analysis, Finite Elem. Anal. Des. 16 (1993) 99–139.
[32] J. Lemonds and A. Needleman, Finite element analysis of shear localization in rate and temperature dependent solids, Mech. Mater. 5 (1986) 339–361.
[33] J. Lubliner, On the thermodynamic foundations of non-linear solid mechanics, Int. J. Non-Linear Mech. 7 (1972) 237–254.
[34] J. Lubliner, On the structure of the rate equations of materials with internal variables, Acta Mech. 17 (1973) 109–119.
[35] J. Lubliner, Plasticity Theory (Macmillan Publishing Company, New York, 1990).
[36] G. Maier, Some theorems for plastic strain rates and plastic strains, Journal de Mécanique 8 (1969) 5.
[37] J. Mandel, Plasticité classique et viscoplasticité, Technical report, Lecture Notes, Int. Centre for Mech. Sci., Udine (Springer, Berlin, 1972).
[38] J.E. Marsden and T.J.R. Hughes, Mathematical Foundations of Elasticity (Prentice-Hall, Englewood Cliffs, NJ, 1983).
[39] J.B. Martin and A.R.S. Ponter, A note on a work inequality in linear viscoelasticity, Quart. Appl. Math. 24 (1966) 161.
[40] T.D. Marusich and M. Ortiz, Modelling and simulation of high-speed machining, Int. J. Numer. Methods Engrg. 38 (1995) 3675–3694.
[41] C. Miehe, Exponential map algorithm for stress updates in anisotropic multiplicative elastoplasticity for single crystals, Int. J. Numer. Methods Engrg. 39 (1996) 3367–3390.
[42] C. Miehe and E. Stein, A canonical model of multiplicative elasto-plasticity. Formulation and aspects of the numerical implementation, Europ. J. Mech. A/Solids 11 (1992) 25–43.
[43] J.J. Moreau, Sur les lois de frottement, de plasticité et de viscosité, C. R. Acad. Sci. Paris 271 (1970) 608–611.
[44] J.J. Moreau, Sur l'evolution d'un système elasto-visco-plastique, C. R. Acad. Sci. Paris 273 (1971) 118–121.
[45] J.J. Moreau, On unilateral constraints, friction and plasticity, in: G. Capriz and G. Stampacchia, eds., New Variational Techniques in Mathematical Physics, Centro Internazionale Matematico Estivo, II Ciclo 1973 (Edizioni Cremonese, Roma, 1974) 175–322.
[46] J.J. Moreau, Application of convex analysis to the treatment of elastoplastic systems, in: P. Germain and B. Nayroles, eds., Applications of Methods of Functional Analysis to Problems in Mechanics (Springer-Verlag, 1976).
[47] A. Needleman, Material rate-dependence and mesh sensitivity in localization, Comput. Methods Appl. Mech. Engrg. 67(1) (1988) 69–85.
[48] M. Ortiz, Topics in constitutive theory for inelastic solids, Ph.D. Thesis, University of California at Berkeley, Berkeley, CA, 1981.
[49] M. Ortiz and J.B. Martin, Symmetry-preserving return mapping algorithms and incrementally external paths: A unification of concepts, Int. J. Numer. Methods Engrg. 28 (1989) 1839–1853.
[50] M. Ortiz, P.M. Pinsky and R.L. Taylor, Operator split methods for the numerical solution of the elastoplastic dynamic problem, Comput. Methods Appl. Mech. Engrg. 39(2) (1983) 137–157.
[51] M. Ortiz and E.P. Popov, Accuracy and stability of integration algorithms for elastoplastic constitutive relations, Int. J. Numer. Methods Engrg. 21 (1985) 1561–1576.
[52] M. Ortiz and J.J. Quigley, Adaptive mesh refinement in strain localization problems, Comput. Methods Appl. Mech. Engrg. 90 (1991) 781–804.
[53] M. Ortiz and E.A. Repetto, Nonconvex energy minimization and dislocation structures in ductile single crystals, J. Mech. Phys. Solids (1998).
[54] M. Ortiz and J.C. Simo, An analysis of a new class of integration algorithms for elastoplastic constitutive relations, Int. J. Numer. Methods Engrg. 23 (1986) 353–366.

[55] D. Pierce, R.J. Asaro and A. Needleman, An analysis of nonuniform and localized deformation in ductile single crystals, Acta Metallurgica 30 (1982) 1087–1119.
[56] M. Ortiz, P.M. Pinsky and K.S. Pister, Numerical integration of rate constitutive equations in finite deformation analysis, Comput. Methods Appl. Mech. Engrg. 40 (1983) 137–158.
[57] P.M. Pinsky, M. Ortiz, and R.L. Taylor, Operator split methods for the numerical solution of the finite-deformation elastoplastic dynamic problem, Comput. Struct. 17(3) (1983) 345–359.
[58] R. Radovitzky and M. Ortiz, Error estimation and adaptive meshing in strongly nonlinear dynamic problems, Comput. Methods Appl. Mech. Engrg. 172 (1999) 203–240.
[59] B. Ramaswami, U.F. Kocks and B. Chalmers, Latent hardening in silver and Ag-Au alloy, Trans. Metall. Soc. AIME 233 (1965) 927.
[60] J.R. Rice, Inelastic constitutive relations for solids: an internal-variable theory and its applications to metal plasticity, J. Mech. Phys. Solids 19 (1971) 433.
[61] J.R. Rice, Continuum mechanics and thermodynamics of plasticity in relation to microscale deformation mechanisms, in: A.S. Argon, ed., Constitutive Equations in Plasticity (MIT Press, Cambridge, MA, 1975) 23–79.
[62] E. Schmid and N. Boas, Kristall. Plastizität (Springer, Berlin, 1961).
[63] J.C. Simo, J.G. Kennedy and S. Govindjee, Non-smooth multisurface plasticity and viscoplasticity. Loading/unloading conditions and numerical algorithms, Int. J. Numer. Methods Engrg. 26 (1988) 2161–2185.
[64] J.C. Simo and T.J.R. Hughes, General return mapping algorithms for rate-independent plasticity, in: C.S. Desai, ed., Constitutive Laws for Engineering Materials: Theory and Applications (Elsevier, 1987) 221–231.
[65] J.C. Simo and M. Ortiz, A unified approach to finite deformation elastoplastic analysis based on the use of hyperelastic constitutive relations, Comput. Methods Appl. Mech. Engrg. 49 (1985) 221–245.
[66] J.C. Simó and R.L. Taylor, Consistent tangent operators for rate independent elasto-plasticity, Comput. Methods Appl. Mech. Engrg. 48 (1985) 101–118.
[67] J.F. Soechting and R.H. Lance, A bounding principle in the theory of work-hardening plasticity, J. Appl. Mech. 36 (1969) 228.
[68] C. Teodosiu, A dynamic theory of dislocations and its applications to the theory of the elastic-plastic continuum, in: J.A. Simmons, ed., Conf. Fundamental Aspects of Dislocation Theory, Vol. 2, Natl. Bureau of Standards Special Publication (Washington, 1969) 837.
[69] F. Tinloi and V. Vimonsatit, Nonlinear analysis of semirigid frames—a parametric complementarity approach, Engrg. Struct. 18(2) (1996) 115–124.
[70] F. Tinloi, Complementarity and nonlinear structural analysis of skeletal structures, Struct. Engrg. Mech. 5(5) (1997) 491–505.
[71] R. Verfürth, A Review of A Posteriori Error Estimation and Adaptive Mesh-refinement Techniques (John Wiley & Sons and B.G. Teubner Publishers, New York, NY, 1996).
[72] R.R. Wakefield and F. Tinloi, Mathematical programming and uniqueness in nonholonomic plasticity. Comput. Struct. 34(3) (1990) 477–483.
[73] G. Weber and L. Anand, Finite deformation constitutive equations and a time integration procedure for isotropic hyperelastic-viscoelastic solids, Comput. Methods Appl. Mech. Engrg. 79 (1990) 173–202.
[74] M.L. Wilkins, Calculation of elastic-plastic flow, in: B. Adler, ed., Methods of Computational Physics 3 (Academic Press, New York, 1964).
[75] G. Friesecke and G. Doltzmann, Implicit time discretization and global existence for a quasi-linear evolution equation with non-convex energy, SIAM J. Math. Anal. 28 (1997) 363–380.